NTNU – Trondheim
Norwegian University of
Science and Technology

Investigation on CO2 Ground-coupled Heat Pumping System with Ejector

Monjur Morshed

Natural Gas Technology
Submission date: July 2015
Supervisor: Trygve Magne Eikevik, EPT

Norwegian University of Science and Technology
Department of Energy and Process Engineering

Monjur Morshed

Investigation on CO_2 Ground-coupled Heat Pumping System with Ejector

Master Thesis

Trondheim, July 2015

Supervisor: Prof. Trygve M. Eikevik

Norwegian University of Science and Technology

Faculty of Engineering Science and Technology

Department of Energy and Process Engineering

NTNU – Trondheim
Norwegian University of
Science and Technology

NTNU
Norwegian University
of Science and Technology

Department of Energy
and Process Engineering

EPT-M-2015-59

MASTER THESIS

for

Student Monjur Morshed

Spring 2015

Investigation on CO_2 ground-coupled heat pumping system with ejector

Undersøkelser av CO_2 varmepumpe med ejektor, koblet mot grunnvarmekilde/sluk

Background and objective

This master thesis is the continual work of the project work ''Energy performance of ground coupled CO_2 heat pump for buildings'', which tries to expand the application of CO_2 heat pump technology to the field of sustainable energy. CO_2 as a natural refrigerant shows great potential in the future refrigeration industry and vast majority of research work is in progress to increase the energy efficiency of CO_2 heat pumps. Ground-coupled heat pump as a sustainable technology is increasingly deployed for heating and cooling application for different types of buildings. This thesis aims to improve the energy efficiency of the concept of CO_2 ground-coupled heat pumping system by introducing a new ejector model. During this master thesis, student should continue to focus on the development of the ground coupled CO_2 heat pump models which could evaluate the energy performance of the system under different conditions. In addition, a new modelica ejector model based on the existed ejector model need to be developed and integrated in heat pump models.

The following tasks are to be considered:

1. Literature review related to the scope of work of the thesis
2. Improve and optimize the developed models by utilizing Modelica.TIL suite and Modelica.building library
3. Develop a new Modelica ejector model based on the existed ejector model and available experimental data
4. Investigate and optimize the seasonal energy performance of CO_2 ground-coupled heat pumping systems at different climatic zones
5. Make a scientific paper based on the main results of the thesis
6. Make suggestion for further work

-- " --

Within 14 days of receiving the written text on the master thesis, the candidate shall submit a research plan for his project to the department.

When the thesis is evaluated, emphasis is put on processing of the results, and that they are presented in tabular and/or graphic form in a clear manner, and that they are analyzed carefully.

The thesis should be formulated as a research report with summary both in English and Norwegian, conclusion, literature references, table of contents etc. During the preparation of the text, the candidate should make an effort to produce a well-structured and easily readable report. In order to ease the evaluation of the thesis, it is important that the cross-references are correct. In the making of the report, strong emphasis should be placed on both a thorough discussion of the results and an orderly presentation.

The candidate is requested to initiate and keep close contact with his/her academic supervisor(s) throughout the working period. The candidate must follow the rules and regulations of NTNU as well as passive directions given by the Department of Energy and Process Engineering.

Risk assessment of the candidate's work shall be carried out according to the department's procedures. The risk assessment must be documented and included as part of the final report. Events related to the candidate's work adversely affecting the health, safety or security, must be documented and included as part of the final report. If the documentation on risk assessment represents a large number of pages, the full version is to be submitted electronically to the supervisor and an excerpt is included in the report.

Pursuant to "Regulations concerning the supplementary provisions to the technology study program/Master of Science" at NTNU §20, the Department reserves the permission to utilize all the results and data for teaching and research purposes as well as in future publications.

The final report is to be submitted digitally in DAIM. An executive summary of the thesis including title, student's name, supervisor's name, year, department name, and NTNU's logo and name, shall be submitted to the department as a separate pdf file. Based on an agreement with the supervisor, the final report and other material and documents must be given to the supervisor in digital format. All relevant data collected and produced during the project shall be delivered to the supervisor on a Memory stick at the end of the project.

☐ Work to be done in lab (Water power lab, Fluids engineering lab, Thermal engineering lab)
☐ Field work

Department of Energy and Process Engineering, January 12th 2015

Prof. Olav Bolland
Department Head

Prof Trygve M. Eikevik
Academic Supervisor
e-mail: Trygve.m.eikevik@ntnu.no

Research Advisor:
PhD-student Zhequan Jin

e-mails
zhequan.jin@ntnu.no

Abstract

After the proposal of CO_2 transcritical cycle in 1980s by Professor Gustav Lorentz, researchers have looked into theoretical and experimental research, as well as commercial system development to improve transcritical system performance to a level similar to that of conventional heat pump systems. Over the years researchers are investigating for newer system concepts with transcritical CO_2 cycle that can be implemented across the globe for different climate conditions. One of the major challenges of CO_2 transcritical cycle is that the system COP is greatly dependent on the gas cooler outlet condition. Thus, application of such systems in wormer climate may result in poor system performance where ambient temperature is relatively high and unstable. However, the temperature of the ground remains comparatively stable and can be utilized as a heat sink to bring down the gas cooler outlet temperature to avoid low cooling performance and large expansion losses. These observations lead the concept of a hybrid system where part of the gas cooler heat is rejected to ambient air and rest to the ground using a ground-coupled heat exchange. Furthermore, incorporating an ejector instead of conventional expansion valve may increase the system performance. It is necessary to evaluate these system alternatives and figure out the maximum borehole length required for such systems to be functional and economically viable.

This thesis investigates the performance of CO_2 ground-coupled ejector cycle to conventional CO_2 transcritical cycle with expansion valve when ambient air temperature constraints the cooling of supercritical CO_2. After a theoretical analysis, the system configurations were implemented in Modelica for further simulation.

Acknowledgement

This thesis has been carried out at Norwegian University of Science and Technology (NTNU), Department of Energy and Process Engineering.

First of all, I owe my deepest gratitude to my supervisor Professor Trygve M. Eikevik for giving me the opportunity to realize this work and for all the instructive guidance. My grateful acknowledgement goes to my research advisor Zhequan Jin, for his weekly meetings, suggestions, information sharing, and unstained help in the duration of this work.

I am also very grateful to Krzystoz Banasiak from SINTEF Energy Research for his valuable information about ejectors and guideline for system configuration and simulation in Modelica.

Further acknowledgement goes to my family for their understanding and support throughout my education in Norway. In addition, I would like to express my gratitude to all my classmates from Natural Gas Technology master program for all the nice moments that we shared together.

Monjur Morshed

Trondheim, July 2015

Table of Contents

List of Figures

List of Tables

1 Introduction

Over the last two decades there has been a major change in heat pumping and refrigeration systems due to emphasis on use of natural refrigerants over the synthetic working fluids which have adverse effect on environment. Among the natural working fluids, use of CO_2 was reinvented by Professor Gustav Lorentz in the late 1980s with a proposal of CO_2 transcritical cycle (CO_2 TRC cycle), and since then theoretical and experimental research, as well as commercial system development, have been carried out to improve transcritical system performance to a level similar to that of conventional heat pump systems. Over the years researchers are investigating for newer system concepts with transcritical CO_2 cycle that can be implemented across the globe for different climate conditions.

This thesis titled "Investigation on CO_2 ground-coupled heat pumping system with ejector", is focused on both theoretical analysis and system simulation of transcritical CO_2 systems by incorporating two different technologies, namely ground couple heat exchangers in the heating side and ejectors to increase system COP. It extends on the concept represented by Jin et al. (2014) at 11th Gustav Lorentzen Conference on Natural Refrigerants.

1.1 Aim and Motivation

One of the major challenges of CO_2 TRC cycle is that the system COP is greatly dependent on the gas cooler outlet condition. Thus, application of such systems in wormer climate may result in poor system performance where ambient temperature is relatively high and unstable. However, the temperature of the ground remains comparatively stable and can be utilized as a heat sink to bring down the gas cooler outlet temperature to avoid low cooling performance and large expansion losses. These observations led the concept of a hybrid system where part of the gas cooler heat is rejected to ambient air and rest to the ground using a ground-coupled heat exchange. Furthermore, incorporating an ejector instead of conventional expansion valve may increase the system performance. It is necessary to evaluate these system alternatives and figure out the maximum borehole length required for such systems to be functional and economically viable.

Use of ejectors in CO_2 TRC cycle is a new technology especially for supermarket refrigeration systems in order to avoid expansion losses. However, the performance of the ejector is greatly dependent on its geometry and design. Although some researchers have proposed models for theoretical CO2 ejector cycle, without experimental data prediction of its behavior cannot be

validated. This thesis utilizes experimental work of a particular ejector geometry for steady state cycle calculation that has been carried out by some recent researchers. Eventually, simulation of different cycle configurations was carried out in Modelica using TIL library.

1.2 Outline of Thesis

In order to perform a satisfactory research on the stated goal and scope of the thesis, the following procedures are taken:

2: CO_2 as a Working Fluid in Heat Pumping Systems

This chapter discusses the properties of CO_2 as a working medium together with a literature review of contemporary research on its heat transfer properties, and system design related to transcritical cycle.

3: Borehole Heat Exchanger Models

A literature review of current research in borehole heat exchanger field is provide in this chapter. The Erdwärmesonden (EWS) model is discussed in details along with the equations used by Modelica Building library.

4: CO_2 Ejector Cycle

Along with a literature review, this chapter discusses limitation of simple model and use of recent experimental results. It also discusses the ejector model in Modelica TIL library and utilization of experimental data for simple steady state calculation of the ejector cycle.

5: Case Study and Solution Approach

This chapter documents the systems considered for analysis along with their respective boundary conditions and governing equations.

6: Results and Discussion

The outcome of the investigations are listed in this chapter with relevant diagrams and discussion.

7: Conclusion

This chapter makes the concluding remarks of this thesis and suggests future work.

2 CO_2 as a Working Fluid in Heat Pumping Systems

As synthetic refrigerants have hazardous environmental consequences, using CO_2 as working fluid for heat pumping systems gained much attention in the last two decades. Although CO_2 has zero GWP and ODP, it is important to compare its properties and heat pump cycles with other refrigerants to validate its use as a working fluid.

In the beginning of this chapter, properties of CO_2 will be discussed, followed by description of reference thermodynamic cycles for transcritical CO_2 heat pump, and a simple analysis of CO_2 transcritical operation. Later part of this chapter will focus on current research on performance of CO_2 heat pumps and development of components used in transcritical cycle.

2.1 Properties of CO_2

For designing a heat pumping system and its components, it is important to know the properties of the working fluids. Compared to other widely used refrigerants, thermodynamic and transport properties of CO_2 are quite different that enable designing of heat pump systems with high COP.

The critical temperature and pressure of CO_2 are 31.1 ˚C and 73.8 bar and triple point temperature and pressure are -56.5˚C and 5.2 bar respectively (Fig. 2.1). It is important to note that critical temperature of CO_2 is very low whereas critical pressure is high compared to other refrigerants. This can be seen from Table 2-1 that lists characteristics and properties of CO_2 and compares these with other working fluids (Lorentzen, 1995; Rieberer, 1998). This low critical temperate of CO_2 puts constraint on the condensing temperature when CO2 systems operate at some subcritical pressure.

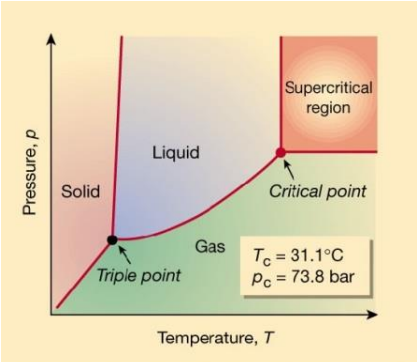

Figure 2.1 Phase diagram of CO_2

Professor Gustav Lorentzen (Lorentzen, 1990) from Norway saw that as an opportunity to operate CO_2 systems in transcritical level, i.e. instead of condensing high pressure CO_2 vapor in a condenser, CO_2 is compressed above its critical pressure where it becomes supercritical fluid and cool it using a gas cooler before it is expanded back to subcritical low-side evaporating pressure (Lorentzen, 1990).

Table 2-1 Characteristics of some refrigerants

	R-744	R-12	R-22	R-134a	R-407C	R-410A	R-717	R-290
ODP/GWP	0/1	1/8500	0.05/1700	0/1300	0/1600	0/1900	0/0	0/3
Flammability/toxicity	N/N	N/N	N/N	N/N	N/N	N/N	Y/Y	Y/N
Molecular mass (kg/kmol)	44	120.9	86.5	102	86.2	72.6	17	44.1
Normal boiling point (˚C)	-78.4	-29.8	-40.8	-26.2	-43.8	-52.6	-33.3	-42.1
Critical pressure (MPa)	7.38	4.11	4.97	4.07	4.64	4.79	11.42	4.25
Critical temperature	31.1	112	96	101.1	86.1	70.2	133	96.7
Reduced pressure	0.47	0.07	0.1	0.07	0.11	0.16	0.04	0.11
Reduced temperature	0.9	0.71	0.74	0.73	0.76	0.79	0.67	0.74
Refrigeration capacity (kJ/m^3)	22545	2734	4356	2868	4029	6763	4382	3907

In his Phd thesis Rieberer (1998) developed property database CO2REF for CO_2 that covers both subcritical and supercritical regions. Some properties of CO_2 were presented by Pettersen (2002) using CO2lib developed by NTNU/SINTEF. Thermophysical data for CO_2 can also be found in (*ASHRAE*, 2001) handbook. By reviewing the available data on CO_2, Span and Wagner (1996) developed a new equation of state where special interest was focused on the description of the critical region and the extrapolation behavior of the formulation. Work by Vesovic et al. (1990) is one of the major references for transport properties of CO2. However, Fenghour, Wakeham, and Vesovic (1998) published improved data for viscosity consistent with the experimental results.

2.1.1 Thermodynamic Properties

Fig. 2.2 (a) shows the vapor pressure curve of CO_2 juxtaposed to that of other refrigerants. It is apparent that CO_2 has much higher vapor pressure compared to other refrigerants, and this characteristic of CO_2 limits the condensing temperature up to 28 ˚C when operated at subcritical level for all practical purposes. Furthermore, as the steepness of CO_2 vapor curve near the

critical temperature is high, temperature variation due to pressure change is less compared to other working fluids. Thus, temperature drop associated with frictional pressure drop in heat exchangers will be less than other refrigerants. This point is further clarified in Fig. 2(b) that for a given phase change temperature variation in temperature with respect to pressure change $(\delta T/\delta p)$is much less for CO_2 though it increases when temperature drops.

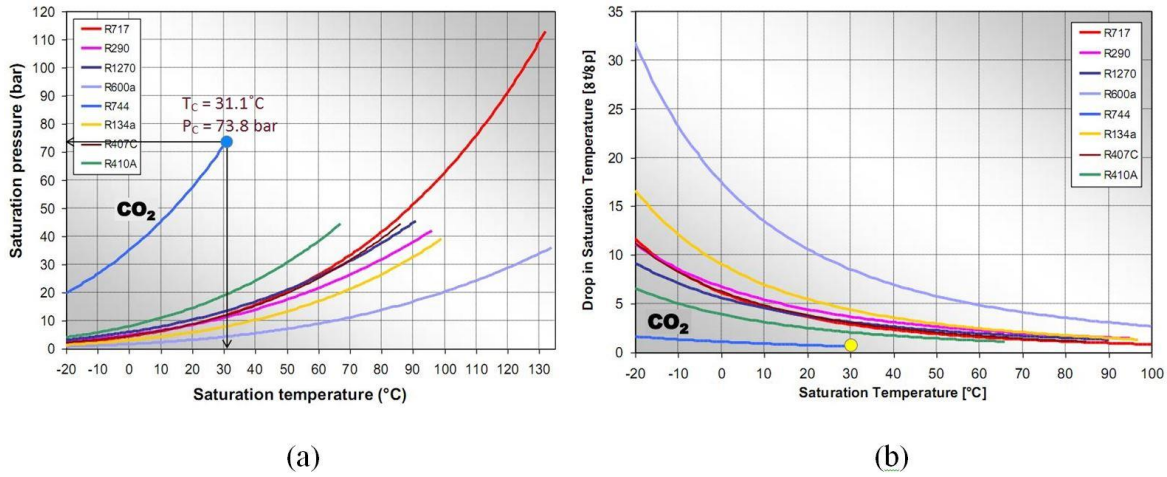

(a) (b)

Figure 2.2 (a) Vapor Pressure curves for different refrigerants, (b) Slope of saturation pressure cure (δT/δp) for refrigerants (Stene, 2014)

In Fig. 2.3 density of CO_2 liquid and vapor is plotted with other working fluids for given temperatures. The density of both liquid and vapor CO_2 sharply changes with respect to temperature near critical point. This behavior along with high vapor pressure at a given temperature (Fig.2 3(b)) compared to others may affect two-phase flow pattern as Pettersen (2002) suggested. Fig 2.4 shows that the density ratio for CO_2 is much smaller compared to other refrigerants. At 0˚C, for instance, the ratio of liquid density (927 kg/m^3) to vapor density (98 kg/m^3) of CO_2 is around 10, whereas for R-410A and R-134a the values are 65 and 89 respectively. One of the consequences of low density ratio of CO_2 is that it gives more homogeneous two-phase flow than other refrigerants (*ASHRAE*, 2001; Pettersen, 2002).

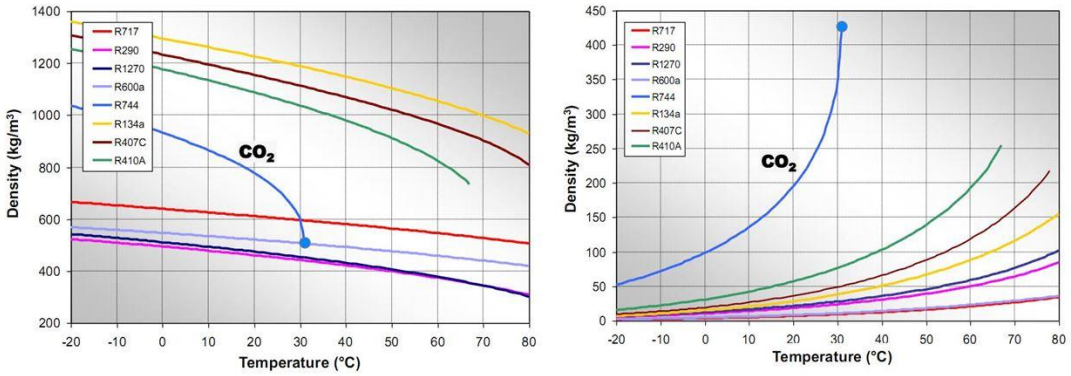

Figure 2.3 (a) Liquid density, (b) Vapour density of CO2 and other refigerants (Stene, 2014)

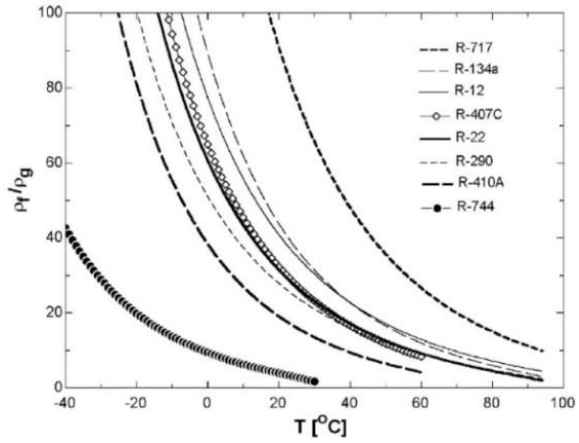

Figure 2.4 Ratio of liquid to vapor density at saturation for refrierants (M. H. Kim, Pettersen, & Bullard, 2004)

Volumetric refrigeration capacity (VRC) is defined as the product of density and latent heat of evaporation, and for CO_2 as vapor density is large compared to other refrigerants for a given evaporating temperature, VRC of CO_2 is also large. Fig. 5 shows that VRC of CO_2 is way above than other working fluids, and it increases with temperature upto maximum at 22˚C. This characteristic of CO_2 is very significant since it indicates that heat pumping systems with smaller compresssors can be built by using CO_2 as refrigerant.

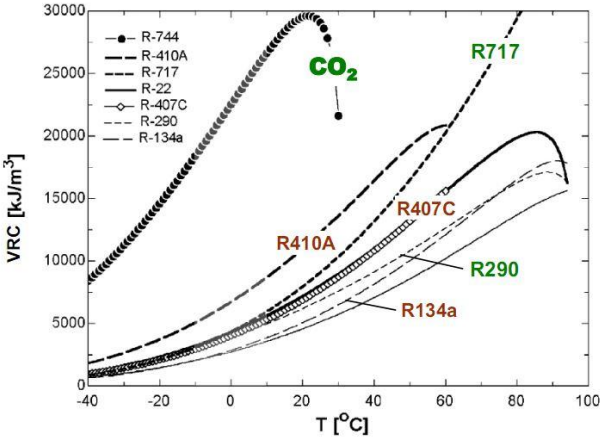

Figure 2.5 Volumetric refrigeration capacities for refrigerants (M. H. Kim, Pettersen, & Bullard, 2004)

In transcritical operation of CO_2, supercritical CO_2 is cooled in a gas cooler, and one of the important parameters for designing this heat exchanger is specific heat at constant pressure (c_p). However, c_p value for CO_2 changes rapidly with temperature, especially near the pseudocritical points (the temperature at which the specific heat becomes a maximum for a given pressure), as mentioned by M. H. Kim, Pettersen, and Bullard (2004)

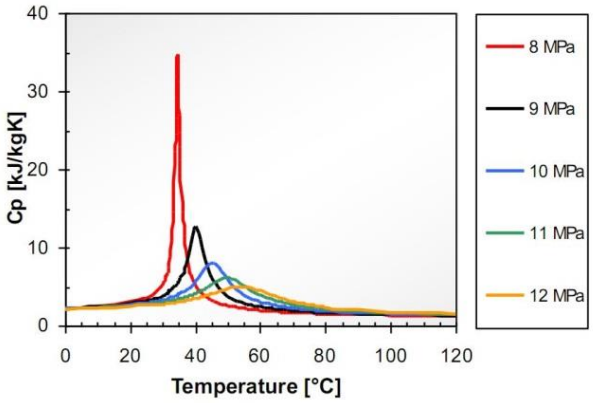

Figure 2.6 Isobaric specific heat of CO2 (Stene, 2014)

Liao and Zhao (2002) proposed an empirical equation to calculate pseudocritical temperature (T_{pseudo}) for pressure (p) ranging between 74 to 140 bars.

$$T_{pseudo} = -122.6 + 6.214p - 0.165p^2 + 0.1773p^{2.5} - 0.0005608p^3 \qquad (2.1)$$

Yang et al. (2006) proposed a different equation to which is also based on pressure –

$$T_{pseudo} = -31.40 + 12.15p - 0.6927p^2 + 0.03160p^3 - 0.000752p^4 \qquad (2.2)$$

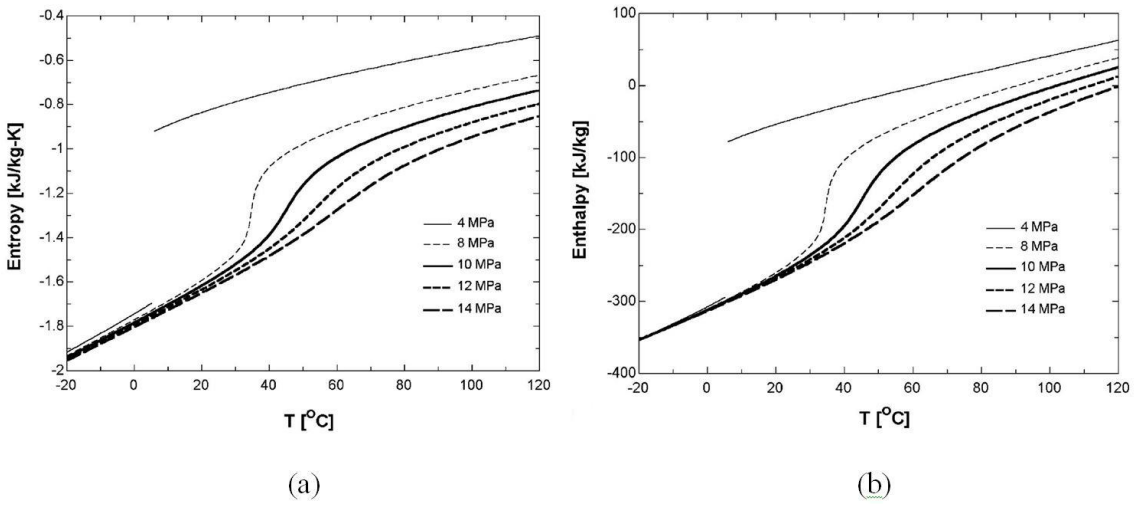

(a) (b)

Figure 2.7 Entropy and enthalpy changes of CO2 in gas cooling process, (a) Entropy change, (b) Enthalpy change (Kim et al., 2003)

Fig. 2.7 shows entropy and enthalpy change of CO_2 during cooling process at different constant pressures; both of these thermodynamic properties show similar behavior. At a constant pressure with decreasing temperature enthalpy and entropy of CO_2 decrease, and the decrease is abrupt near critical temperature. Furthermore, with lower pressure abrupt decrease is less pronounced.

2.1.2 Transport Properties

Thermal conductivity and dynamic viscosity are two important properties for a fluid when it comes to determination of heat transfer and pressure drop associated with its flow. In Fig. 2.8 (a) and (b) show thermal conductivity and viscosity of CO_2 at different pressure levels (form subcritical to supercritical pressure) with decrease in temperature. During cooling, both of the properties vary less for a particular pressure up to near critical temperature. However, irrespective of pressure, cooling below critical temperature results in increased value for both properties. Moreover, at near critical pressure both properties show abrupt changes when temperature is close to critical point. According to Pettersen (2002), thermal conductivity of both liquid and vapor CO_2 is 20 and 60% higher than that of R-134a, respectively. While the viscosity of vapor CO_2 is comparable, viscosity of liquid CO_2 is 40% of R-134a liquid viscosity.

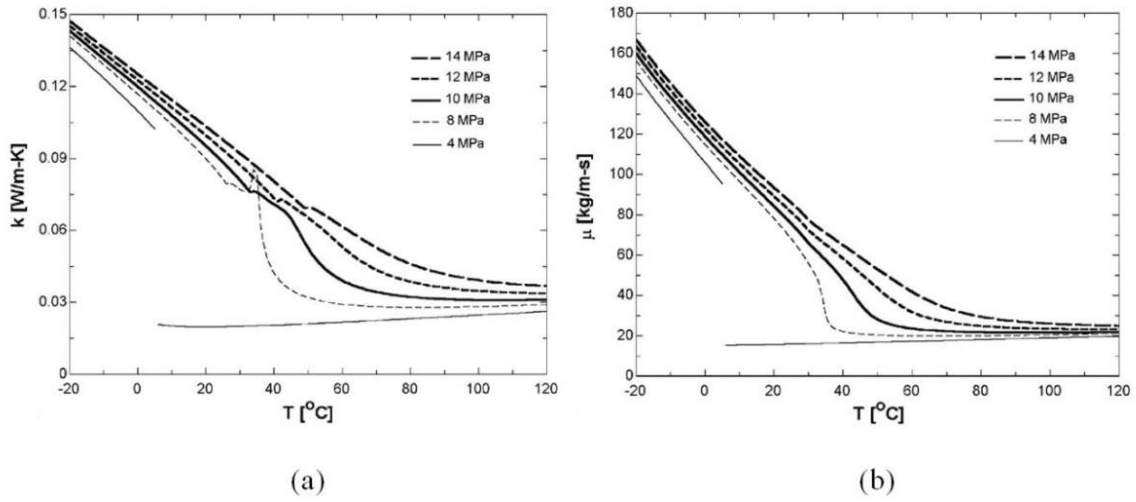

Figure 2.8 Transport properties of CO2, (a) Thermal conductivity, (b) Dynamic viscosity (Kim et al., 2003)

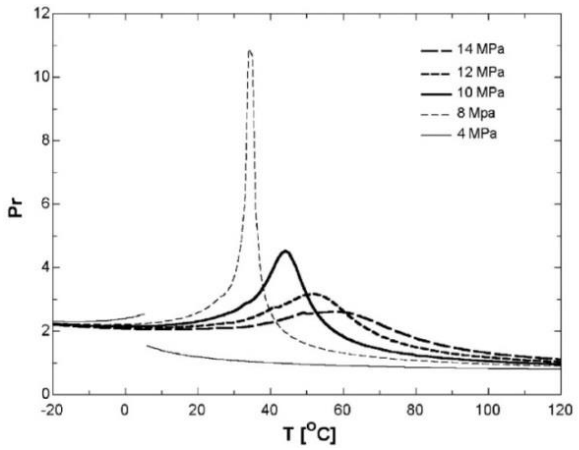

Figure 2.9 Prandtl number of CO2 (M. H. Kim et al., 2004)

Fig. 2.9 depicts the Prandtl number as a function of temperature. It can be seen that for a given pressure maximum value of Prandtl number occurs near pseudocritical temperature associated with corresponding specific heat, and with increase in pressure the value decreases (M. H. Kim et al., 2004).

2.1.3 Properties of the supercritical CO_2 with lubricants

Lubrication plays an important role in compressor as lubricants are responsible for smooth operations of the moving parts, noise reduction, sealing, and cooling friction surface. However,

lubricants get mixed with refrigerants end up in the heat exchangers. Falex test (Falex Corporation, USA) showed that in order for good to bad, performance of lubricants containing 10% CO_2 are: Polyalkylene glycol (PAG) > Polyol ester (POE) > Alkylbenzene > Polyalphaolefin (PAO). Thus, PAG/CO_2 has best lubrication performance.

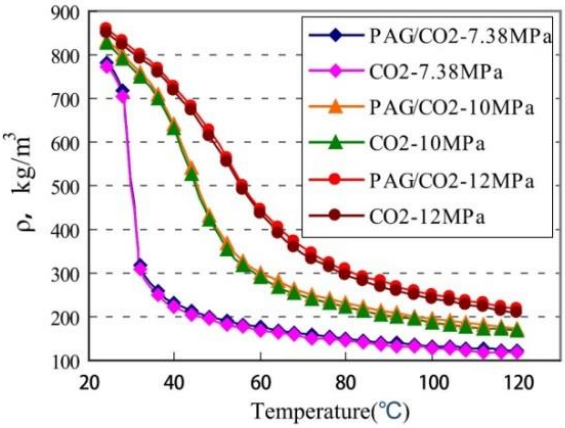

Figure 2.10 Density variation of CO2 and PAG/CO2 mixtire with temperature (Ma, Liu, & Tian, 2013)

Mutual solubility with refrigerant is an important measure to choose lubricants. Fig. 2.10 shows that for a given temperature, the solubility of CO_2 increases as pressure increases, and at the same pressure, it decreases with the increase of temperature. Hence, at low temperature, the solubility of CO_2 in PAG is high, and the mixture has a poor lubrication performance. In contrast, at high temperature, the solubility is low, giving good lubrication performance. Thus it can be seen, the lower the pressure as well as the higher the temperature is the better lubrication performance PAG/CO_2 has (Y. Ma et al., 2013).

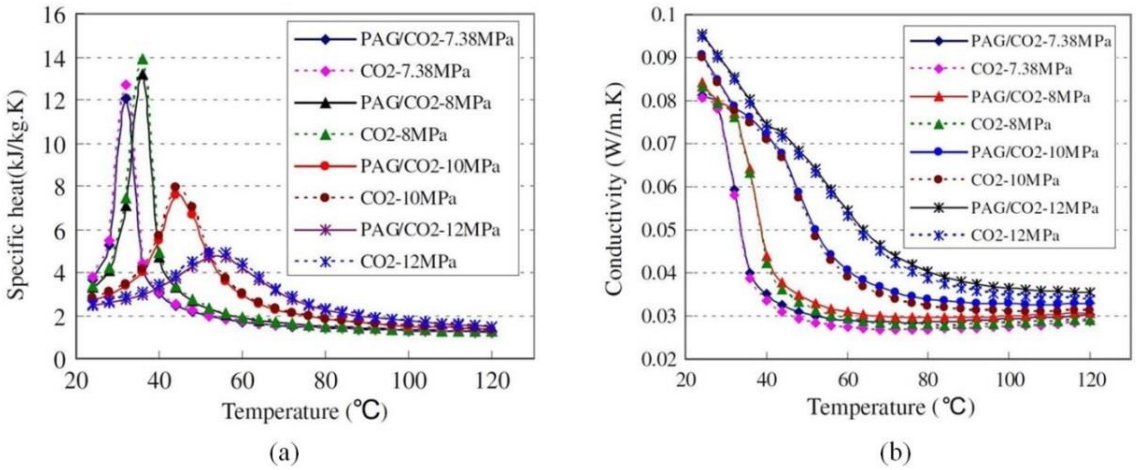

Figure 2.11 (a) Specific heat, (b) thermal conductivity of supercritical pure CO2 and PAG/CO2 mixture (Ma, Liu, & Tian, 2013)

Jensen and Jackman (1984) carried out both specific heat and thermal conductivity experiment on lubricant- refrigerant mixture containing 10% lubricant, and found the conductivity of mixture increased by less than 3%.Fig 2.11(a) shows that the constant pressure specific heat of supercritical CO_2 is slightly higher than that of mixture, and the change trend that specific heat of mixture changes with the change of temperature and pressure is basically consistent with the pure one. That is to say, trace amounts of lubricant has little effect on constant pressure specific heat of supercritical CO_2, so the change trend of mixture specific heat cannot be determined by it. From Fig. 2.11(b), the thermal conductivity of supercritical CO_2 is slightly worse than that of mixture containing trace amounts of PAG. Thus trace amounts of lubricant have little effect on the thermal conductivity of supercritical CO_2.(Ma, Liu, & Tian, 2013)

2.2 CO_2 Transcritical Cycle for Heat Pumps

As mentioned in section 1.1, in a transcritical heat pumping system the working fluid is compressed above its critical pressure and the supercritical gas is cooled down by exchanging heat with another medium in gas cooler. It is important to note that, gas cooling is a sensible cooling process where the difference between the inlet and out let temperature of the gas cooler is much higher than conventional (subcritical cycle) heat pumps. Thus, CO_2 transcritical cycle can be used for heating application that requires a large temperature increase such as domestic hot water.

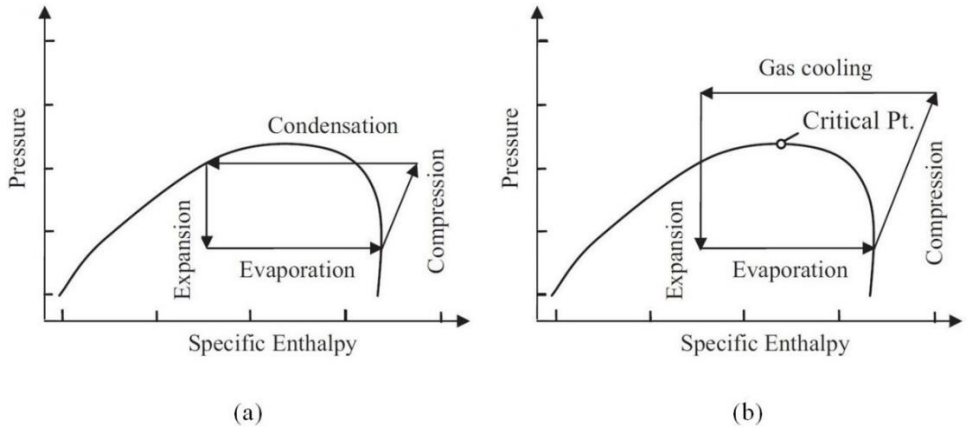

Figure 2.12 P-h diagram showing: (a) subcritical cycle and (b) transcritical cycle (Austin & Sumathy, 2011)

2.2.1 Thermodynamic Cycles for CO_2 Heat Pump

According to Neksa (2002) CO_2 systems in subcritical operation compete very well with respect to energy efficiency with systems using other refrigerants. As thermodynamic cycle analysis of CO2 systems in subcritical operation is same as for other working fluids, in the following sections thermodynamic analysis of transcritical cycle will be discussed in detail.

2.2.1.1 Modified Lorentz Cycle

For conventional refrigeration cycles, reversed Carnot cycle is used as theoretical reference cycle. However, for the transcritical CO_2 cycle heat rejection occurs in gliding temperature in gas cooler, but heat absorption takes place at constant temperature as in a conventional cycle. Klöcker, Flacke, and Schmidt (1998) suggested that for analyzing transcritical cycle the modified Lorentz cycle should be adopted. Fig. 2.13 depicts Lorentz cycle in T-s diagram, where $T_m$the mean temperature of the hot fluid and heat source temperature is T_0 (both the temperatures are in Kelvins).

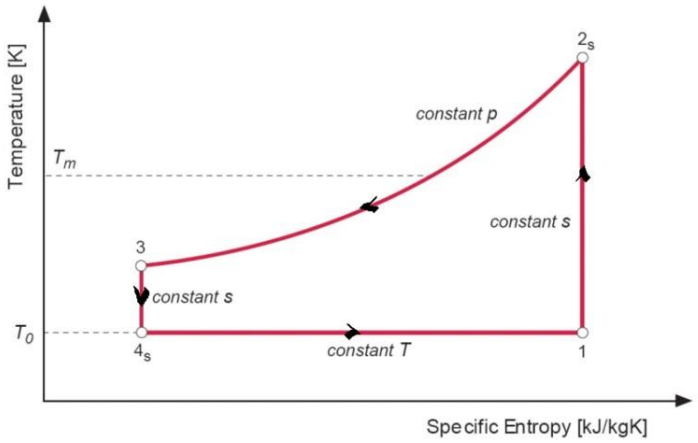

Figure 2.13 Modified Lorentz cycle in T-s diagram (Klöcker et al., 1998)

The modified Lorentz cycle consists of the following processes –

4s – 1 : Heat absorption at constant temperature and pressure

1 – 2 : Reversible adiabatic compression

2s – 3 : Heat rejection at constant pressure and gliding temperature

3 – 4s : Reversible adiabatic expansion

The coefficient of performance for the modified Lorentz cycle (COP_{LZ}) is defined as

$$COP_{LZ} = \left(\frac{T_m}{T_m - T_0}\right) \tag{2.3}$$

The Lorentz efficiency is the thermodynamic efficiency for the transcritical heat pump cycles, and it is defined as

$$\eta_{LZ} = \left(\frac{COP_{HP}}{COP_{LZ}}\right) \tag{2.4}$$

2.2.1.2 Ideal and Real Lorentzen Cycle

Generally the ideal Evans- Perkins cycle is used as the ideal reference cycle for conventional heat pumps, however, Halozan and Ritter (1994) proposed to use the ideal Lorentzen cycle as the ideal reference cycle for the transcritical CO_2 heat pump cycle. Fig. 2.14 shows the cycle in a T-s diagram.

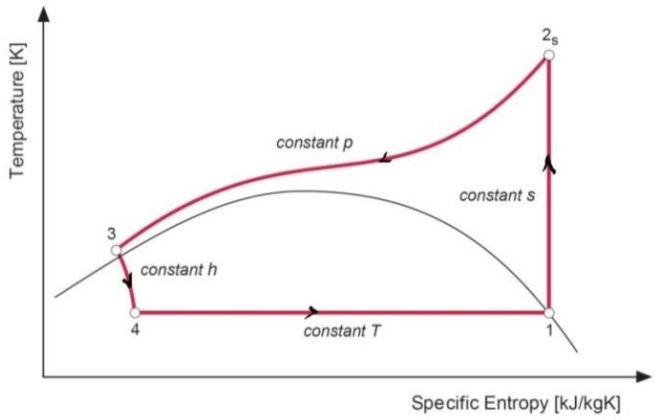

Figure 2.14 Ideal Lorentzen cycle for CO2 in a T-s diagram (Halozan & Ritter, 1994)

The cycle consists of the following processes-

4 – 1 : Heat absorption at constant subcritical temperature and pressure

1 – 2s : Reversible adiabatic compression to supercritical pressure

2s – 1 : Heat rejection at constant pressure and gliding temperature

3 – 4 : Isenthalpic (adiabatic) expansion

However, the real CO_2 transcritical cycle or Lorentzen cycle deviates from ideal Lorentzen cycle due to process irreversibility. The real cycle consists of the following processes-

4 – 1' : Non-isobaric (i.e. non-isothermal) heat absorption

1' – 1 : Non-isobaric superheating of the suction gas

1 – 2 : Irreversible polytropic non-adiabatic compression to supercritical pressure

2 – 3 : Non-isobaric supercritical heat rejection at gliding temperature

3 – 4 : Non-isenthalpic (non-adiabatic) expansion

In Fig. 2.15 real transcritical CO_2 heat pump cycles are illustrated both T-h and p-h diagrams where irreversibilities in the cycle are evident.

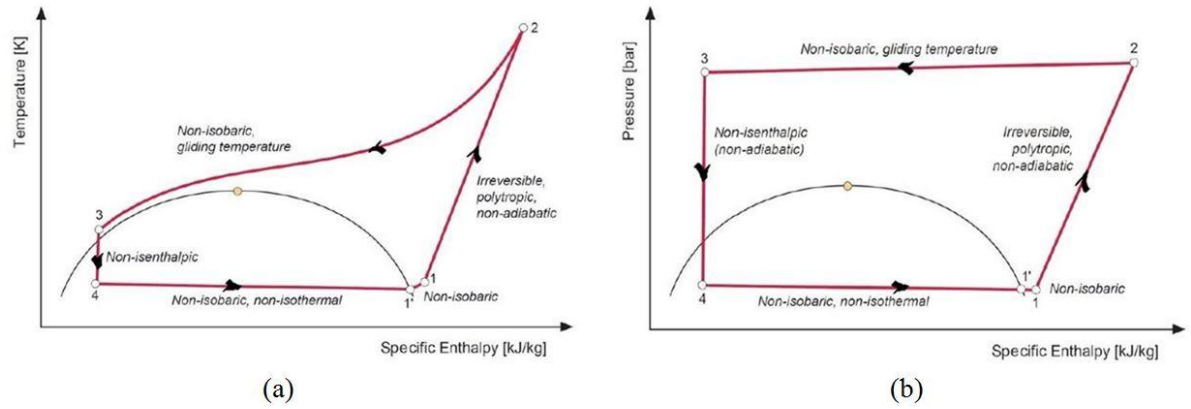

(a) (b)

Figure 2.15 Real transcritical cycle for CO2 heat pump cycles in T-h and p-h diagrams (Halozan & Ritter, 1994).

2.2.2 CO_2 Transcritical Cycle Analysis

In this section of the chapter a simple thermodynamic model of transcritical CO_2 cycle will be presented together with its pressure drop and heat transfer characteristics. The assumptions are-

- Steady state operation of the system
- Kinetic and potential energy associated with streams are neglected
- Compressor and all heat exchangers operate adiabatically
- Heat loss connected to piping is neglected
- Isenthalpic expansion process

Heating capacity and Coefficient of Performance (COP) are the two parameters that are used to characterize the performance of a heat pump. It is important to mention at this point that the energy performance of the transcritical cycle greatly depends on the out let temperature of the gas cooler which can be seen evidently by looking at the T-h or T-s diagram of the Lorentzen cycle without any calculation.

Due to steady state assumption, in all devices mass flow rate in and out are equal. Hence,

$$\dot{m}_i = \dot{m}_o = \dot{m} \tag{2.5}$$

Heading capacity and COP for heating and cooling can be calculated using the following equations –

$$\dot{Q}_{capacity} = \dot{m} \times \left(h_{gc,i} - h_{gc,o}\right) \tag{2.6}$$

$$COP_{heating} = \frac{h_{gc,i} - h_{gc,o}}{h_{copm,o} - h_{comp,i}} \tag{2.7}$$

$$COP_{cooling} = \frac{h_{ev,o} - h_{ev,i}}{h_{comp,o} - h_{comp,i}} \tag{2.8}$$

In this analysis it is also assumed that both the gas cooler and the evaporator are concentric-tube counter-flow heat exchangers with CO_2 flowing in the inner tube and water (secondary fluid) flows in the outer.

2.2.2.1 Gas Cooler

Energy balance for the gas cooler gives the following equations –

$$\dot{Q}_{gc} = \dot{m} \times \left(h_{gc,i} - h_{gc,o}\right) \tag{2.9}$$

$$\dot{Q}_{gc} = \dot{m}_w \times c_{p,w} \times \left(T_{gc,w,o} - T_{gc,w,i}\right) \tag{2.10}$$

As cooling of supercritical CO_2 takes place with gliding temperature, heat transfer in the longitudinal direction of the concentric tube may also be significant other than heat transfer in radial direction which is generally the case. However, in a study Asinari, Cecchinato, and Fornasieri (2004) showed that in a gas cooler longitudinal heat transfer is negligible even in regions with greatest temperature gradient. The heat transfer rate $\dot{Q}_{gc}$, can be defined based on the overall heat transfer coefficient and the temperature difference between the two fluids using the logarithmic mean temperature difference method.

$$\dot{Q}_{gc} = UA \times \frac{\left(T_{gc,i} - T_{gc,w,o}\right) - \left(T_{gc,o} - T_{gc,w,i}\right)}{ln(T_{gc,i} - T_{gc,w,o})/(T_{gc,o} - T_{gc,w,i})} \tag{2.11}$$

where, $U$and A are overall heat transfer coefficient and heat transfer coefficient, respectively.

2.2.2.2 Evaporator

Heat transfer and energy balance equations for the evaporator are same as gas cooler with appropriate subscripts.

$$\dot{Q}_{ev} = \dot{m} \times \left(h_{ev,o} - h_{ev,i}\right) \tag{2.12}$$

$$\dot{Q}_{ev} = \dot{m}_w \times c_{p,w} \times \left(T_{ev,w,i} - T_{ev,w,o}\right) \tag{2.13}$$

$$\dot{Q}_{ev} = UA \times \frac{\left(T_{ev,w,i} - T_{ev,o}\right) - \left(T_{ev,w,o} - T_{ev,i}\right)}{ln(T_{ev,w,i} - T_{ev,o})/(T_{ev,w,o} - T_{ev,i})} \tag{2.14}$$

2.2.2.3 Compressor

The mass flow rate in the compressor can be determined using the following equation –

$$\dot{m} = V_s \times \lambda \times N \times \rho_{suction} \tag{2.15}$$

where, V_s is the swept volume of the compressor, N is the speed of the compressor, and λ is the volumetric efficiency of the compressor.

Generally the volumetric efficiency and isentropic efficiency of the compressor depend on the pressure ration between high and low pressure sides. The following equations can be used to calculate them when pressure ration is known (Oritz, Li, & Groll, 2003).

$$\lambda = 0.9207 - 0.0756 \times r + 0.0018 \times r^2 \tag{2.16}$$

$$\eta_{is} = -0.26 + 0.7952 \times r - 0.2803 \times r^2 + 0.0414 \times r^3 - 0.0022 \times r^4 \tag{2.17}$$

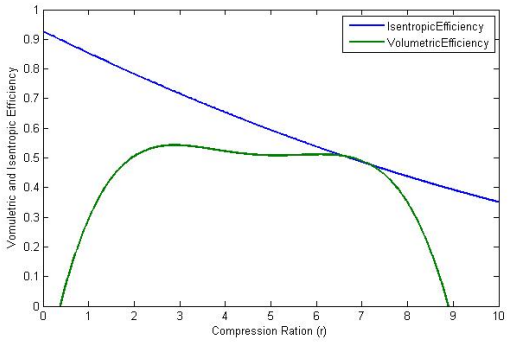

Figure 2.16 Isentropic and Volumetric Efficiency of the compressor according to equation (15) and (16)

2.2.2.4 Expansion Valve

Ass the expansion process is isenthalpic, the energy equation becomes the following –

$$h_{exp,i} = h_{exp,o} \tag{2.18}$$

2.2.2.5 Heat Transfer and Pressure Drop Characteristics of CO_2

Cooling of supercritical CO_2 has been investigated by several researchers in order to find heat transfer correlations for horizontal channels and micro channels. Yoon et al. (2003) conducted experimental studies on heat transfer coefficient of CO_2 flowing in a 7.73mm inner diameter horizontal tube. Based on the experimental results a new correlation was proposed, and Oh and Son (2010) showed that the correlation developed by Yoon et al. (2003) is one of the most accurate for micro channels. The correlation developed is shown in Eq. (2.19) where two set of parameters are listed for temperature greater than T_{pseudo} and temperature less than or equal to $T_{pseudo,}$ and all the parameters are calculated using bulk temperature T_b.

$$Nu_b = aRe_b^c Pr_b^d \left(\frac{\rho_{pseudo}}{\rho_b}\right)^n \tag{2.19}$$

for $T_b > T_{pseudo}$:	a = 0.14	c = 0.69	d = 0.66	n = 0
for $T_b \leq T_{pseudo}$:	a = 0.013	c = 1.0	d = -0.05	n = 1.6

Experimental results show that (Fig. 2.17) during cooling process heat transfer coefficient gradually increased and reached a maximum value before it declined. One of the reasons for that being specific heat varies abruptly near pseudocritical temperature. Furthermore, the maximum value of the heat transfer coefficient decreases with increase in pressure.

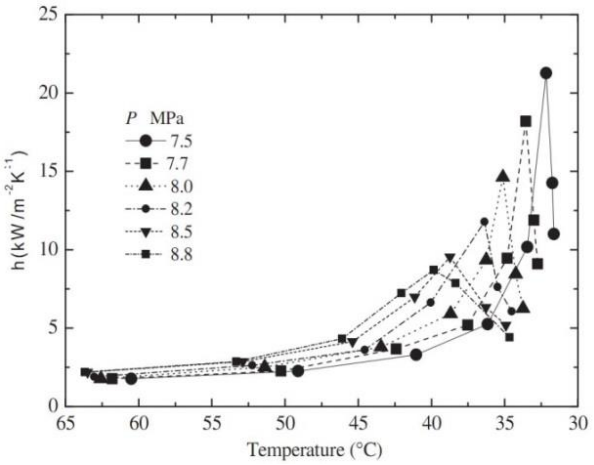

Figure 2.17 Variable heat transfer coefficient with different temperatures (Yoon et al., 2003)

In their experimental study of evaporation heat transfer of CO_2, Bredesen, Hafner, Pettersen, Neksa, and Aflekt (1997) found the heat transfer coefficient of CO_2 was higher and pressure droop was less compared to that of synthetic refrigerants respectively. At high mass flow and low evaporating temperature, convective boiling is the main heat transfer model. On the other hand, when mass flow is low and evaporating temperature is high, nucleate boiling is the main heat transfer mode (Bredesen et al., 1997).

2.3 Researches on CO_2 Transcritical Cycle

As heat pumping, air conditioning, or refrigeration systems are essentially the same except the desired output and operating temperature, this section will discuss recent research on CO_2 transcritical cycle irrespective of application area. However, it is important to keep in mind that COP and capacity are defined differently for cooling and heating systems.

2.3.1 CO_2 Transcritical Cycle with a suction line heat exchanger

One of the major modifications in CO_2 transcritical cycle is the addition of a suction gas heat exchanger (SGHX) that cools the gas cooler outlet vapor by exchanging heat with the discharge vapor out of the evaporator (Fig. 2.18).

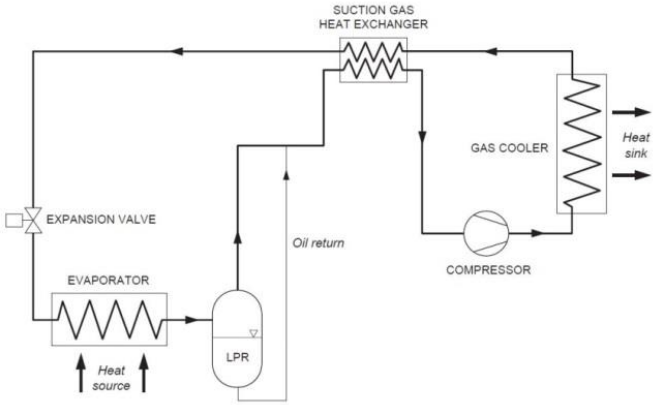

Figure 2.18 CO2 transcritical cycle operations with a suction gas heat exchanger (Lorentzen, 1990)

In a comparison, Jiang and Ma (2009) showed that the heating COP of transcritical CO_2 cycle with a SGHX is 5-10% higher a cycle without it when the inlet temperature of CO_2 was 20˚C for the SGHX. In their research, Chen and Gu (2005) found that as SGHX effectiveness increases, optimum pressure decreases and COP increases. S. G. Kim, Kim, Lee, and Kim (2005) simulated the effect of SGHX to optimize its size with respect to gas cooler pressure and found that under a certain gas cooler pressure, COP improved up to 4% on average as SGHX length was increased. It is important to note that adding a SGHX leads to higher capital cost, and decision is made with tradeoff between investment and energy performance of the system. The impact of the SGHX on COP and heating capacity can be summarized as –

- It evaporates liquid droplets in the suction gas resulting in slight increase in compressor efficiency
- It superheats the outlet gas of the evaporator leading to lower vapor density and higher temperature at the inlet of the compressor. Thus, reduces CO_2 mass flow rate slightly
- It increase the discharge temperature of the compressor, and it results in increase of heating capacity
- As it reduces the temperature before expansion valve, higher specific evaporation capacity can be achieved due to small flash-gas formation
- It reduces the optimum gas cooler pressure
- It increase both cooling and heating COP of the system

2.3.2 Optimum gas cooler pressure

One of the key attributes of CO_2 transcritical cycle is that temperature and pressure are independent of each other during supercritical CO_2 cooling process. While pressure in the gas cooler is kept constant, supercritical CO_2 rejects heat at falling temperature unlike conventional condensation process (Fig. 2.19).

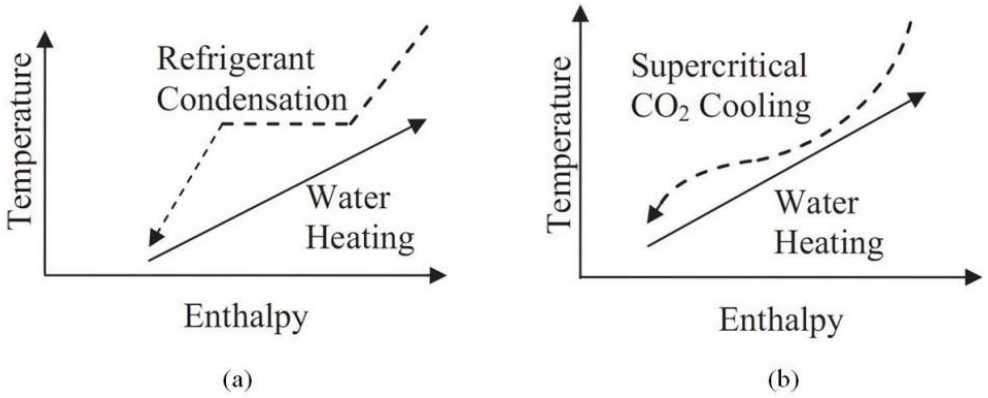

Figure 2.19 (a) Heat rejection in conventional heat pump (b) heat rejection in CO2 transcritical cycle at falling temperature (Austin & Sumathy, 2011).

The shape of the cooling curve of supercritical CO_2 depends on the gas cooler pressure, and the slope of the T-h diagram represents the inverse of the specific heat capacity.

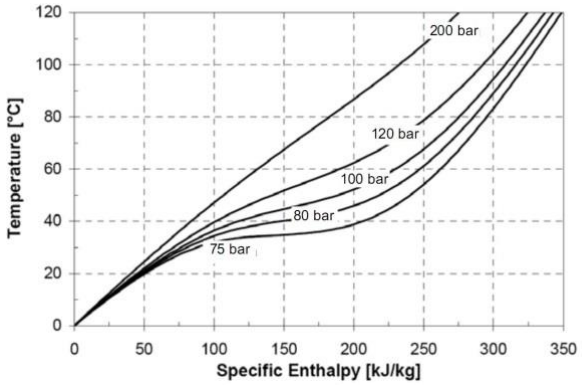

Figure 2.20 Temperature-enthalpy curves (isobars) for supercritical CO2 (Stene, 2014)

For a supercritical pressure and temperature close to critical point of CO_2 (73.8 bars, 31.1˚C) value of specific heat capacity becomes very large (Fig.2.6) and the T-h curve has a sway-

backed shape – 75 bar isobar curve in Fig. 2.20. Consequently change in temperature during cooling in situ condition is very small. With increase in gas cooler pressure the isobars become straighter showing less and less sway-backed behavior. At very high pressure (~ 200 bars) the isobar is almost a straight line, which implies that the specific heat capacity is almost constant and remains invariant with falling temperature. In order to have better heat transfer and high heat rejection in gas cooler, the T-h curve of CO_2 should behave identically to that of secondary fluid such as air or water. However, heating curve of air or water is relatively straight during heating from 0 to 100 ˚C due to their respective constant specific heat over this temperature range. This shows that for effective heat transfer process gas cooler pressure should be high in order to get best temperature fit between Supercritical CO_2 and secondary fluid. Furthermore, high gas cooler pressure is achieved in expense of high compression work. Thus, it directly affects the COP of the heating system.

Keeping this as a motivation many researchers have conducted both theoretical and experiment work to predict the optimum pressure for the gas cooler that would give best COP of the heating system with less compressor work and high heat rejection at the gas cooler. Research about the high-side pressure optimization based on thermodynamic cycle simulation and experiment can be found from Liao, Zhao, and Jakobsen (2000), Sarkar, Bhattacharyya, and Gopal (2004), Chen and Gu (2005), W. Yang, Fartaj, and Ting (2005), Cavallini, Cecchinato, Corradi, Fornasieri, and Zilio (2005), Agrawal, Bhattacharyya, and Sarkar (2007), S. C. Kim, Won, and Kim (2009), Srinivasan, Sheahen, and Sarathy (2010), Zhang, Fan, Wang, and Shen (2010); and proposed optimized pressures are listed in Table 2-2. It is noteworthy that Zhang et al. (2010) proposed a novel correlation-free on-line optimal control method for CO_2 transcritical refrigeration systems by dynamic numerical simulation.

Table 2-2 Literature list of optimum gas cooler pressure control equation (temperatures and pressures are in ˚C and bar respectively)

Authors	Control Equation (Transcritical CO_2 cycle with expansion valve)
Kauf	$P_{opt} = 2.6T_{amb} \approx 2.6T_{gc,out} + 7.54$ $T_{gc,out} = T_{amb} = 2.9$ $35 < T_{amb} < 50;\ 91 < P_{opt} < 130$
Liaonet et al.	$P_{opt} = (2.78 - 0.0157T_{evp})T_{gc,out} + (0.381T_{evp} - 9.34)$ $-10 < T_{evp} < 20;\ 30 < T_{gc,out} < 60;\ 71 < P_{gc,out} < 120$
Chen and Gu	$P_{opt} = 2.304T_{amb} + 19.29$ $T_{gc,out} = -0.0015269T_{amb}^2 - 0.028866T_{amb} + 7.7126$ $-10 < T_{evp} < 10;\ 35 < T_{gc,out} < 50;\ 80 < P_{gc,out} < 135$ $P_{opt} = 2.68T_{amb} + 0.975 = 2.68T_{gc,out} - 6.797$ $T_{gc,out} = T_{amb} + 2.9$ $-10 < T_{evp} < 10;\ 35 < T_{gc,out} < 50;\ 80 < P_{gc,out} < 135$
Sarkar et al.	$P_{opt} = 4.9 + 2.256T_{gc,out} - 0.17T_{evp} + 0.002T_{gc,out}^2$ $-10 < T_{evp} < 10;\ 35 < T_{gc,out} < 50$
Kim et al.	$P_{opt} = 1.938T_{gc,out} + 9.872$ $25 < T_{gc,out} < 45;\ 75 < P_{gc,out} < 135$
Authors	Control Equation (Transcritical CO_2 cycle with ejector)
Sarkar et al.	$P_{opt} = 22.7 + 0.21T_{evp} + 1.06T_{gc,out} - 0.0094T_{evp}T_{gc,out} + 0.0213T_{gc,out}^2$ $-45 < T_{evp} < 5;\ 30 < T_{gc,out} < 60$
Eibel and Henjak	$P_{opt} = 1.6T_{gc,out} + 30$ $35 < T_{amb} < 50;\ 88 < P_{gc,out} < 120$

2.3.3 CO_2 transcritical cycle with two-stage compression

As two-stage compression is carried out by intermediate cooling, worked required to compress the refrigerant to desired optimum pressure is less together with reduced compressor outlet temperature unlike single stage compression. Furthermore, volumetric loss in the compressors could be reduced in absence of leakage due to great pressure differential, and higher isentropic efficiency of the compressors could be achieved because of low pressure ratios. However, the investment cost for such systems will be higher for the addition of one more compressor unit.

Cavallini et al. (2005) tested the cooling performance of a two-stage compression transcritical experimental system at different intercooler temperatures, and they found improved cooling COP by 21.1% compared to basic transcritical cycle. Flash intercooling is an alternative means of cooling the refrigerant between compression stages in which the inter-stage CO2 temperature is reduced by mixing with expansion vapor in a flash tank (Austin & Sumathy, 2011). Fig. 2.21 shows the system schematic and cycle diagram of a transcritical CO_2 heat pump incorporating flash intercooling. In their research Agrawal et al. (2007) determined that, unlike other methods of intercooling, two-stage compression with flash intercooling decreased the COP compared to that of an analogous system with single stage compression. This is due to the fact that mass flow rate through the second stage compressor increases significantly. Though the specific work of compression in the second stage is reduced, actual compression work in the second stage increases. Intermediate pressure was found to have little impact on COP (Agrawal et al., 2007).

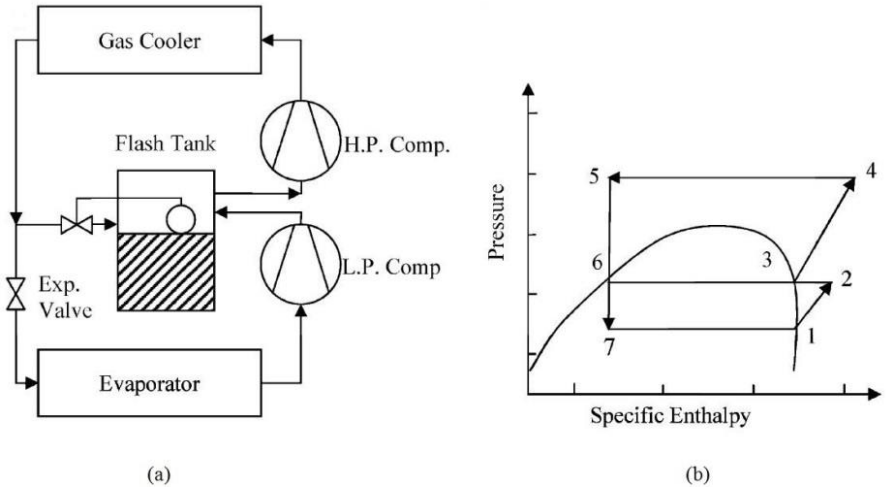

Figure 2.21 Transcritical CO2 heat pump with intercooling: (a) schematic diagram, and (b) cycle p-h diagram (Austin & Sumathy, 2011)

2.3.4 CO_2 transcritical cycle with ejector

One of the downsides of the CO_2 transcritical cycle compared to other working fluids is the expansion losses associated with it. In a transcritical cycle, the greater pressure difference results in greater expansion losses, thus making work recovery more feasible and beneficial. In order to reduce expansion losses two basic cycle modifications, namely- ejector expansion and expander work recovery are proposed by a number of researchers. In this section transcritical

CO_2 cycle with ejector will be discussed briefly. In chapter 4, thermodynamic model of ejector will be discussed together with the model used in Modelica TIL library.

One of the biggest advantages of the ejector over expanders is that it does not contain mechanical moving parts, thus energy does not get dissipated due to friction. Kornhauser (1990) first proposed the ejector-expansion cycle as shown in Fig. 2.22. The basic principle is that the high pressure CO_2 from the gas cooler enters the nozzle of the ejector where its velocity is increased and pressure is decreased. This decreased pressure draws CO_2 vapor from the evaporator into the ejectors mixing chamber where the pressure increases. A diffuser is utilized to increase CO_2 pressure while also lowering the velocity. CO_2 then enters a liquid–vapor separator from which vapor is drawn into the compressor and liquid re-enters the evaporator. As a consequence the inlet pressure of the compressor is increased, thus compressor work is reduced as it operates with low pressure ration.

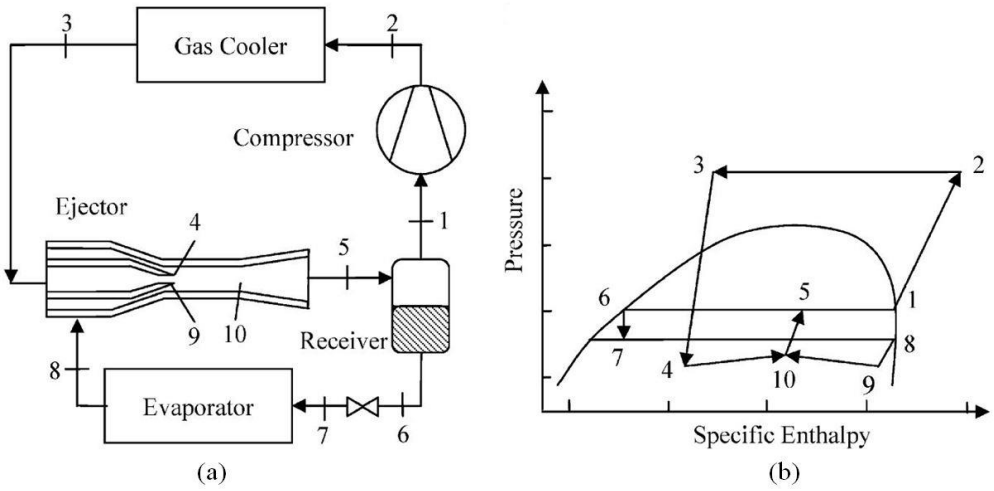

Figure 2.22 Transcritical CO2 heat pump cycle with ejector: (a) system schematic and (b) cycle p-h diagram (Sarkar, 2008)

2.3.5 CO2 transcritical cycle with expander

As mentioned earlier, use of expanders is proposed to reduce expansion losses and recover some work during expansion process. In a theoretical study by W. Yang et al. (2005) showed that an expander produced a 50% decrease in exergy loss compared to conventional expansion valves, resulting in a 30% improvement in system exergy efficiency. The expander reduced the optimum gas cooler pressure also and led to a 33% higher cooling COP. Ma et al. (2013) performed a comparison study with expander using CO_2 and R134a. The summery of their work is listed in Table 2-3.

Table 2-3 Comparison of expander systems using CO2 and R134a as working fluids (expander inlet condition: 40 ˚C, 100 bars; outlet condition: 5 ˚C)

Working fluid	Expansion ration of expander	Compression ratio of compressor	The ratio of expansion work to compression work
CO2	2.637	2.015	0.3789
R134a	16.45	2.84	0.1556

As expansion ration for CO_2 is 2.6 unlike R134a for which the value is higher than 16, it matches the compression ratio, thus it is easier to connect compressor with an expander coaxially in CO_2 systems. Furthermore, the recovered expansion work compared to compressor work is 37% in CO2 system which is two and half times higher than R134a. J. L. Yang, Ma, and Liu (2007) made a theoretical comparison between direct and indirect coupling of the expander and compressors in a transcritical CO_2 cooling system with dual compression. The investigation compared three configurations: (i) expander directly driving the high pressure compressor (DCHP); (ii) expander directly driving the low pressure compressor (DCLP); (iii) expander indirectly driving the low pressure compressor with optimized intermediate pressure (DCOP). Schematic diagrams of the three methods of energy transfer are shown in Fig. 2.23. The systems were also compared to single-stage compression systems with an expansion valve and with an expander. The results of the simulation are presented in Table 2-4. The best performance was achieved by the DCHP system. The DCOP system performed slightly worse. The DCLP system performed worse than a system with single stage compression system and expander. Optimum inter stage pressure was predicted to be much greater than the geometric mean pressure, which is typically used as the optimum intermediate pressure in a subcritical two stage compressor. (Austin & Sumathy, 2011)

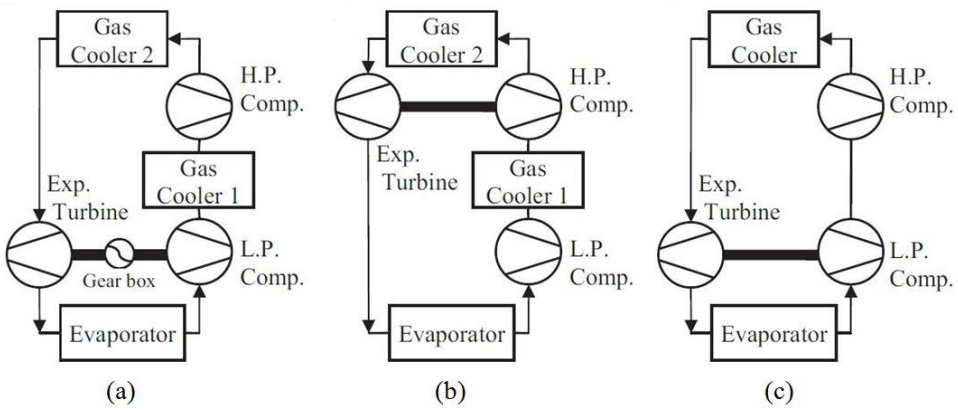

Figure 2.23 Three methods of transferring work recovered from an expansion turbine: (a) indirect low pressure drive with optimized intermediate pressure; (b) direct high pressure drive; (c) direct low pressure drive (Austin & Sumathy, 2011).

Table 2-4 Results of simulation comparing methods of transferring energy recovered from an expansion turbine

Cycle (Tev = 5C, Tgc,o = 40 C	COP	Optimum high pressure (bar)	Intermediate pressure (bar)
Single compression, expansion valve	2.418	100.4	-
Single compression, expander	3.211	96.14	-
DCOP	4.396	96.14	82.62
DCHP	3.521	101.3	80.9
DCLP	3.163	96.2	47.97

2.4 Researches on CO_2 Transcritical Cycle Heat Exchangers

As overall performance of CO2 transcritical cycle depends on mutual interaction among the cycle components, researchers performed exergy analysis to figure out which component holds the greatest potential for overall improvements of cycle performance. A study by Robinson and Groll (1998) showed that the expansion valve suffers the most irreversibilities followed in order by the compressor, gas cooler and evaporator. W. Yang et al. (2005) also found that the most exergy loss occurred in the expansion valve, but concluded that the next greatest contribution to exergy loss depended on operating conditions. In contrast to them Sarkar, Bhattacharyya,

and Gopal (2005) concluded that the compressor had greatest exergy loss, followed in order by the gas cooler, evaporator and finally the expansion valve.

As heat exchangers play an important role in transcritical cycle performance, many research works have been done regarding heat transfer and heat exchanger design for CO_2. In their work Goodman, Fronk, and Garimella (2011) mentioned that the ratio between CO_2 and secondary fluid heat transfer coefficients significantly influence the overall heat transfer coefficient of the heat exchanger. Generally $h_{air} < h_{CO_2}$ and $h_{water} > h_{CO_2}$. Consequently in a water coupled heat exchanger the overall heat transfer coefficient is more sensitive to the CO_2 heat transfer coefficient; h_{CO_2} is the primary factor which determines overall heat transfer coefficient. On the other hand in an air coupled heat exchanger air heat transfer coefficient is the primary factor that determines the overall heat transfer coefficient. In their investigation, Pettersen, Hafner, Skaugen, and Rekstad (1998) found that by increasing the contact area between the refrigerant and the heat exchanger surface, microchannel tubes can reduce the overall size of a heat exchanger for a given heating or cooling capacity together with capability of withstanding high operating pressure. Yin, Bullard, and Hrnjak (2001) modeled microchannel gas cooler with two configurations. In the model, CO_2 flowed through microchannel tube-banks, while air was maintained in cross-flow conditions. Each tube bank consisted of ten or more parallel microchannel tubes connected to a header at each end. In the first test, additional tube-banks were added in the plane perpendicular to the airflow (thus increasing the frontal area of the heat exchanger); in the second test, tube-banks were aligned in the direction the air flow, one behind the other, as shown in Fig. 2.24. In the first test, the model showed an increase in heating capacity from one to three sets of tube-banks. More than three tub-banks produced marginal increase in heat capacity. In second configuration, increase inn number of tube banks resulted in increase in heating capacity and decreased temperature approach (difference between CO_2 outlet temperature and secondary fluid inlet temperature).

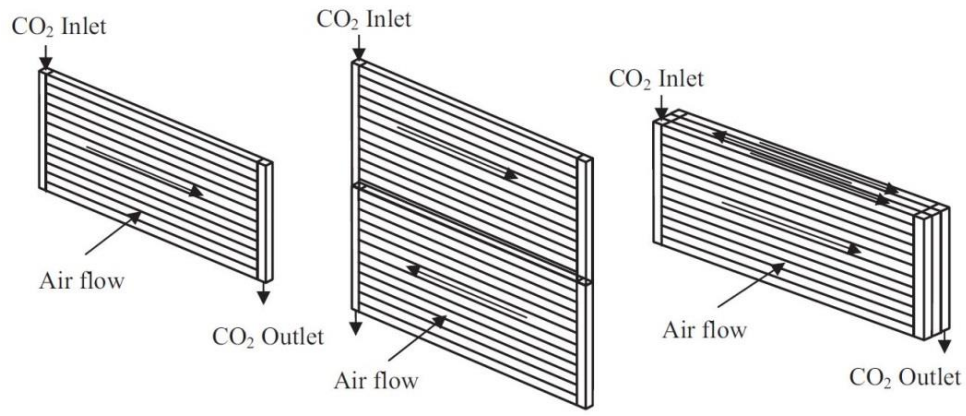

Figure 2.24 Heat exchanger tube-bank configuration for microchannel gas cooler (Austin & Sumathy, 2011)

Bendaoud, Ouzzane, Aidoun, and Galanis (2010) analyzed the performance of finned tube evaporators with CO_2 and found that pressure drop of CO_2 through the evaporator is less than with other refrigerants. Use of microchannel heat exchangers as evaporator was investigated by several authors like (Yun, Kim, & Park, 2007), M. H. Kim and Bullard (2001), and it was shown that the use of a microchannel heat exchanger as the evaporator improves the performance of a transcritical CO_2 heat pump system. In an evaporator alignment and orientation of the slabs also impact the performance as simulation by Yun et al. (2007) indicates. Fig. 2.25 shows two arrangements that were tested, and it was found that two slabs of microchannel tubes arranged in a V-shaped showed better heat transfer capacity than two than two slabs arranged in series with respect to airflow.

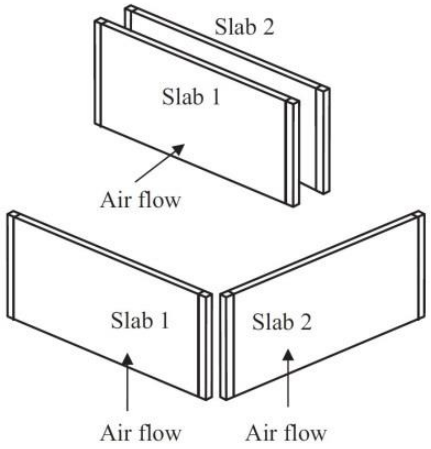

Figure 2.25 Heat exchanger slab configuration for microchannel evaporator (Austin & Sumathy, 2011)

3 Borehole Heat Exchanger Models

In order to provide space heating and cooling as well as domestic hot water in residential and commercial buildings, ground coupled heat pump (GCHP) systems use ground as heat source or sink. Though GCHPs have attractive advantages of high efficiency and environmental friendliness, successful operation of these systems depend on ground heat exchangers (GHE) where heat is extracted from or rejected to the ground via a closed loop using pure water or antifreeze (secondary fluids). The GHEs commonly used in the GCHP systems typically consist of high-density polyethylene (HDPE) pipes which are installed in either vertical boreholes (called vertical GHE) or horizontal trenches (horizontal GHE). The present chapter represents a literature review of vertical GHE or borehole heat exchanger (BHE) models.

BHE configurations may include one, tens, or even hundreds of boreholes, each containing one or double U-tubes through which heat exchange fluid is circulated (Fig. 3.1(a)). Typical U-tubes have a diameter in the range of 19–38 mm and each borehole is normally 20–200 m deep with a diameter ranging from 100 mm to 200 mm. Generally the annulus of the borehole is filled with grout to prevent contamination of ground water. Fig. 3.1(b) shows the schematic of a BHE.

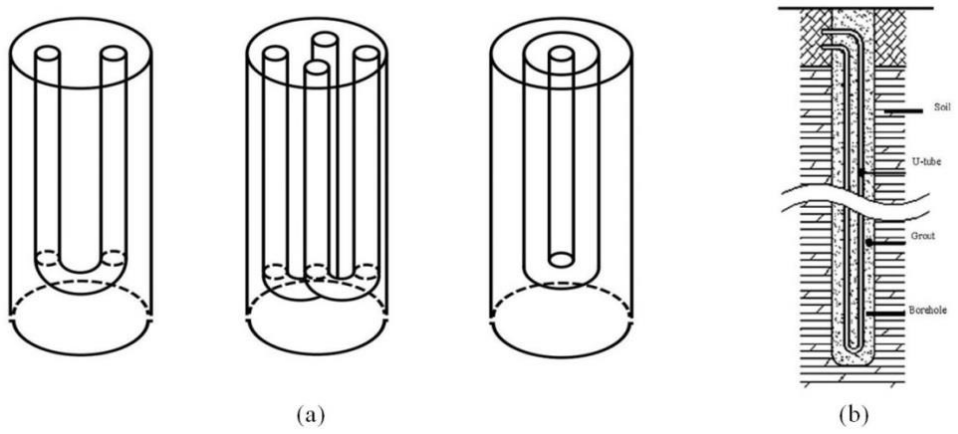

Figure 3.1 (a) Commonly used BHE configurations; from left to right, single U-tube, double U-tube, and concentric tubes (b) schematic of borehole heat exchanger (He, 2012; H. Yang, Cui, & Fang, 2010)

The time required for the secondary fluid to travel inside the tubes ranges from one minute and half to twenty five minutes. Consequently there is a delay in temperature response. On the other hand, the undisturbed ground temperature profile along the depth of the borehole is not uniform.

Typically temperature varies along first ten meters from the surface due to solar radiation and ambient air temperature. Together with these the heat transfer process in BHE also depends on ground thermal properties, ground water flow, and building loads over a long lifespan of several or even tens of years (H. Yang, Cui, & Fang, 2010).

The heat transfer process may usually be analyzed in two separated regions, namely the solid soil/rock outside the borehole and the region inside the borehole, including the grout, the U-tube pipes and the circulating fluid inside the pipes. In the former region heat conduction must be treated as a transient process so that the temperature on the borehole wall can then be determined for any instant on specified operational conditions. The later region is sometimes analyzed as being steady- state or quasi-steady-state and sometimes analyzed as being transient. These two separate analyses must be interlinked on the borehole wall.(H. Yang et al., 2010)

3.1 Classification of the Borehole Models

According to He (2012), depending on the methodology BHE models can be divided into four categories –

1. Analytical models
2. Steady state models
3. Response factor models
4. Discretized numerical models

According to H. Yang et al. (2010) , BHE heat transfer models can be categorized into two types depending on the region of application of the models –

1. Heat transfer models applied outside of the borehole
2. Heat transfer models applied inside the borehole

Table 3-1 Summary of the current ground coupled heat exchanger models

	Model	Methods	Thermal	Boundary
	Kelvin's line source	Infinite line source	Yes	No
	Cylindrical source	Infinite cylindrical source	Yes	No
Outside borehole	Eskilion's source solution	Combination of numerical and analytical methods	Yes	Yes
	Finite line-source solution	Analytical methods	Yes	Yes
	Short time-step model	Numerical methods	Yes	Yes
	Model	Methods	Thermal interference between U-tube pipes	Heat flux along depth
	One-dimensional model (equivalent pipe)	-	No	No
Inside borehole	Two-dimensional model	-	Yes	No
	Quasi-three-dimensional model	-	Yes	Yes

Table 3-1 gives the summary of the models that have been developed over the year by different researchers. Detail information about these models can be found in He (2012) and H. Yang et al. (2010). In this chapter vertical BHE EWS model will be discussed in details followed by the description of the borehole model used in Modelica.Buildings library.

3.2 Vertical BHE EWS Model

The Erdwärmesonden (EWS) model was developed in 1997 by Huber and Wetter for double U-tube BHEs in order to improve the modeling of transient behavior and reducing the simulation time compared to other ground source models. The EWS-model uses a combination of analytical and numerical methods where one dimensional heat equation in cylindrical coordinates is solved using the Crank-Nicholson algorithm. The equation can be expressed as follows –

$$\frac{\partial^2 T}{\partial r^2} + \frac{\partial T}{\partial r} - \frac{1}{\alpha}\frac{\partial T}{\partial r} = 0 \tag{3.1}$$

In order to solve Eqs. 3.1, the BHE is divided into different layer with variable distances in radial direction (Fig. 3.2).

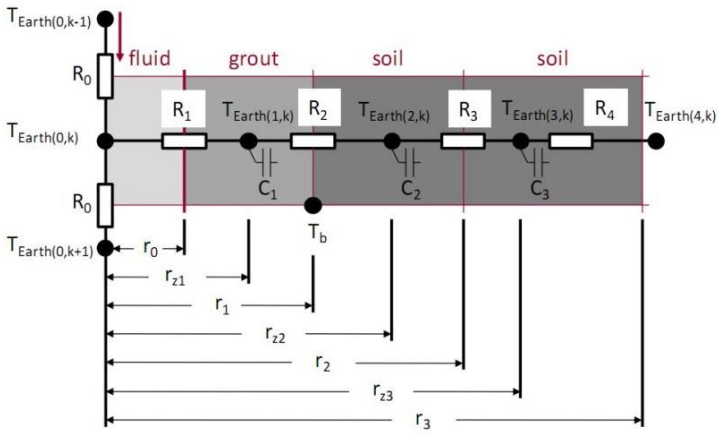

Figure 3.2 Diagram of different layers with variable distances in radial direction of the BHE (He, 2012).

$$\left.\begin{aligned} r_0 &= {}^{D_{in}}/_{2} = inner\ radius\ of\ the\ pipe \\ r_1 &= {}^{D_b}/_{2} = radius\ of\ the\ borehole \\ for\ j \geq 2: r_j &= r_{j-1} + (r_m - r_1)\left(\frac{1-f}{1-f^{m-1}}\right) r^{j-2} \end{aligned}\right\} \tag{3.2}$$

where r_m and f are the maximum radius of the simulation area and the grid factor respectively. The grid factor is defined in the following way –

$$f = \frac{r_{j+1} - r_j}{r_j - r_{j-1}} \tag{3.3}$$

In the above equations, j is the index of calculation point, r_j is the radius on calculation point j.

Discretization of Eqs. 3.1 according to Crank-Nicholson method gives –

$$\begin{aligned} T_{n+1,j} - \frac{dt}{2}\frac{L_j}{C_j}\left(T_{n+1,j-1} - T_{n+1,j}\right) - \frac{dt}{2}\frac{L_{j+1}}{C_j}\left(T_{n+1,j+1} - T_{n+1,j}\right) \\ = T_{n,j} + \frac{dt}{2}\frac{L_j}{C_j}\left(T_{n,j-1} - T_{n,j}\right) + \frac{dt}{2}\frac{L_{j+1}}{C_j}\left(T_{n,j+1} - T_{n,j}\right) \end{aligned} \tag{3.4}$$

where n and j are the indices for time step and radial step respectively. The conductance L and the heat capacity C inside the borehole depends on the type of BHEs. The conductance and heat capacity are defined as –

$$L = \frac{1}{R} = \frac{\dot{Q}}{\Delta T}$$
$$C = c_p \rho V \tag{3.5}$$

where R is the thermal resistance. The following equations express the thermal capacity and thermal resistance –

$$C_{1,j} = C_{grout} = (c_p \rho)_{grout} \pi (r_1^2 - 4r_0^2) dl$$
$$for\ i \geq 2:\ \ C_{i,j} = (c_p \rho)_{soil\_j} \pi (r_i^2 - r_{i-1}^2) dl \tag{3.6}$$

$$R_1 = \frac{1}{4} \frac{1}{2\pi dl} \left(\frac{1}{\alpha r_0} + \frac{1}{k_{grout}} ln \frac{r_1 - r_{z1}}{r_0} \right)$$
$$R_2 = \frac{1}{2\pi dl} \left(\frac{1}{k_{grout}} ln \frac{r}{r_{z1}} + \frac{1}{k_{soil}} ln \frac{r_{z2}}{r_1} \right) \tag{3.7}$$
$$for\ i \geq 3:\ \ R_i = \frac{1}{2\pi dl} \frac{1}{k_{soil}} ln \frac{r_{zi}}{r_{z(i-1)}}$$

In the vertical direction, the BHE is divided into layers with equal distances (Fig. 3.3).

$$dl = \frac{Borehole\ length}{DimAxi} \tag{3.8}$$

The fluid temperature is calculated from the energy balance from the upward and downward flowing fluid in each vertical layer. The Temperature of the fluid is then used as the boundary condition of the simulation of the heat transfer in the radial direction from the fluid to the ground as described above.

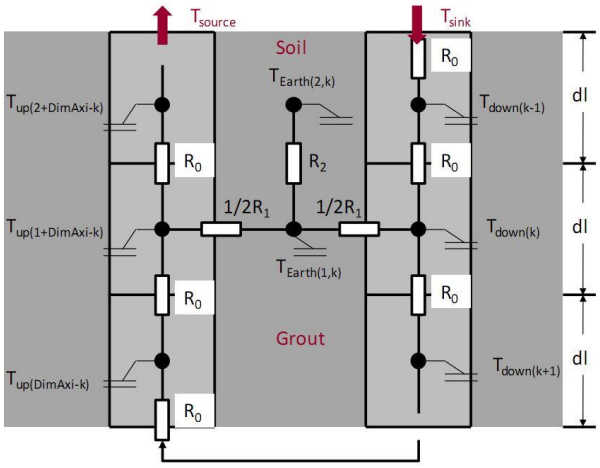

Figure 3.3 Diagram of different layers with equal distance in vertical direction of the BHE(He, 2012).

The energy balance equations for each element are the followings –

$$T_{down(k,n)} = T_{down(k,n-1)} + \left(T_{down(k-1,n)} - T_{down(k,n-1)}\right)\left(\frac{L_0 dt}{mc_p}\right) + \left(T_{Earth(k,n-1,1)} - T_{down(k,n-1)}\right)\left(\frac{L_1 dt}{2mc_p}\right) \tag{3.9}$$

$$T_{up(k,n)} = T_{up(k,n-1)} + \left(T_{up(k-1,n)} - T_{up(k,n-1)}\right)\left(\frac{L_0 dt}{mc_p}\right) + \left(T_{Earth(1+DimAxi-k,n-1,1)} - T_{up(k,n-1)}\right)\left(\frac{L_1 dt}{2mc_p}\right) \tag{3.10}$$

where L_0 is given by –

$$L_0 = c_{p,f}\dot{m} = 2\pi r_0^2 v \rho_f c_{p,f} \tag{3.11}$$

and the boundary condition are –

$$\left.\begin{array}{c} T_{down(0,n)} = T_{sink} \\ T_{up(0,n)} = T_{down(DimAxi,n)} \\ T_{source} = T_{up(DimAxi,n)} \end{array}\right\} \tag{3.12}$$

By solving these equations in the direction of flow, the temperature of the fluid can be calculated.

3.3 Borehole Heat Exchanger Model in Modelica.Buildings library

The borehole heat exchanger consists on a single U-tube which is vertically discretized into n_{seg} elements of height $h = h_{bor}/n_{seg}$. Each segment contains a model for the heat transfer in the borehole, for heat transfer in the soil and for the far-field boundary condition.

The heat transfer in the borehole is computed using a convective heat transfer coefficient that depends on the fluid velocity, a heat resistance between the two pipes, and a heat resistance between the pipes and the circumference of the borehole. The heat capacity of the fluid, and the heat capacity of the grout, is taken into account. All thermal mass is assumed to be at the two bulk temperatures of the down-flowing and up-flowing fluid.

The heat transfer in the soil is computed using transient heat conduction in cylindrical coordinates for the spatial domain $r_{bor} \leq r \leq r_{ext}$. In the radial direction, the spatial domain is discretized into n_{hor} segments with uniform material properties. Thermal properties can be specified separately for each horizontal layer. The vertical heat flow is assumed to be zero, and there is assumed to be no ground water flow.

The far-field temperature, i.e., the temperature at the radius r_{ext}, is computed using a power-series solution to a line-source heat transfer problem. This temperature boundary condition is updated every t_{sample} seconds.

The initial far-field temperature $T_{ext,start}$, which is the temperature of the soil at a radius r_{ext}, is computed as a function of the depth $z > 0$. For a depth between $0 \leq z \leq z_0$, the temperature is set to $T_{ext,0,start}$. The value of z_0 is a parameter with a default of 10 meters. However, there is large variability in the depth where the undisturbed soil temperature starts. For a depth of $z_0 \leq z \leq h_{bor}$, the temperature is computed as –

$$T^i_{ext,start} = T_{ext,0,start} + \left(z^i - z_0\right)\left(\frac{dT}{dz}\right) \tag{3.13}$$

with $i \in \{1,2,\dots,n_{ver}\}$, where the temperature gradient $\left({}^{dT}/_{dz}\right) \geq 0$ is a parameter. As with z_0, there is large there is large variability in $\left({}^{dT}/_{dz}\right) \geq 0$. The default value is set to 1 Kelvin per 100 meters. For the temperature of the grout, the same equations are applied, with $T_{ext,0,start}$ replaced with $T_{fil,0,start}$, and $T^i_{ext,start}$ replaced with $T^i_{fil,start}$. The default setting uses the same temperature for the soil and the filling material.

4 CO_2 Ejector Cycle

This chapter deals with simulation of transcritical CO_2 cycle using Modelica TIL Suit package and Modelica.Buildings library. In addition to a borehole heat exchanger, an ejector is added to the transcritical CO_2 heat pump cycle to evaluate the system performance under different operating conditions. The beginning part of the chapter discusses thermodynamic analysis ejector cycle followed by system simulation of heat pump cycle.

4.1 Thermodynamic Analysis of Transcritical CO_2 Heat Pump Cycle with Ejector

After the first proposal of ejector cycle by Kornhauser (1990), a number of researchers have done both theoretical and experimental study on the topic. While Li and Groll (2005) modeled a modified ejector cycle which was designed to adjust the vapor quality at the evaporator inlet and aid steady state operation, Deng, Jiang, Lu, and Lu (2007) focused on the importance of entrainment ratio for optimized performance. Sarkar (2008) theoretically analyzed the use of an ejector in a transcritical CO_2 heat pump for simultaneous heating and cooling.

4.1.1 Basic Structure of Ejectors

An ejector three main parts, namely suction chamber, misxing chamber, and diffuser section (Fig. 4.1). High pressure gas from the gas cooler side called motive stream expands in the motive nozzle, thus its velocity is increased. With high at the motive nozzle exit, motive stream entrains low pressure suction stream (secondary stream) from the evaporator into the misxing section. The two streams mix in the mixsing section and become one stream followed by increase in pressure in the diffuser section.

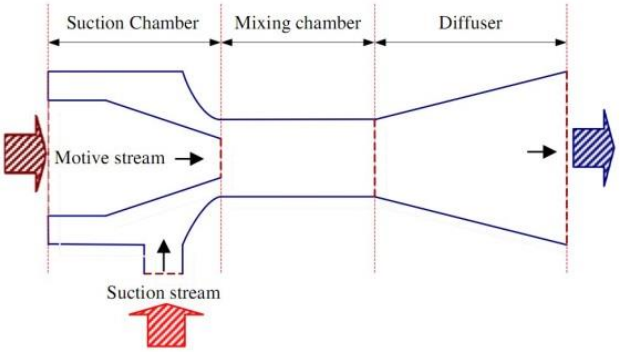

Figure 4.1 Structural sketch of an ejector (Sun & Ma, 2011)

Two performance parameters associated with ejectors are entrainment ratio and pressure list ratio (PLR). They are defined as the following (Sarkar, 2008) –

$$Entrainment\ ratio, \mu = \frac{mass\ of\ secondary\ flow}{mass\ of\ motive\ flow} = \frac{\dot{m}_s}{\dot{m}_m} \quad (4.1)$$

$$Pressure\ Lift\ Ratio, PLR = \frac{static\ pressure\ at\ diffuser\ exit}{static\ pressure\ at\ secondary\ flow\ inlet} \quad (4.2)$$

4.1.2 Mathematical Model of Transcritical Ejector Cycle

The mathematical model of transcritical ejector cycle presented in this chapter will closely follow the model proposed by Sarkar (2008), Li and Groll (2005), Ahammed, Bhattacharyya, and Ramgopal (2014) . The cycle schematic and the p-h diagram are shown in Fig. 4.2, and the following assumptions are made for the ejector cycle –

- Pressure drop in the heat exchangers and connecting pipes is negligible
- The Refrigerant condition at the evaporator outlet is saturated
- The vapor stream and the liquid stream out of the separator are saturated
- The flow is isenthalpic through expansion valve
- Both the motive and the suction stream reach the same pressure at the inlet of the constant area mixing section of the ejector. There is no mixing between the two streams before the constant area mixing section
- The expansion efficiencies of the motive stream and suction stream are given constants, so as the diffuser section efficiency
- Kinetic energy of the refrigerant at the ejector inlet and outlet are negligible

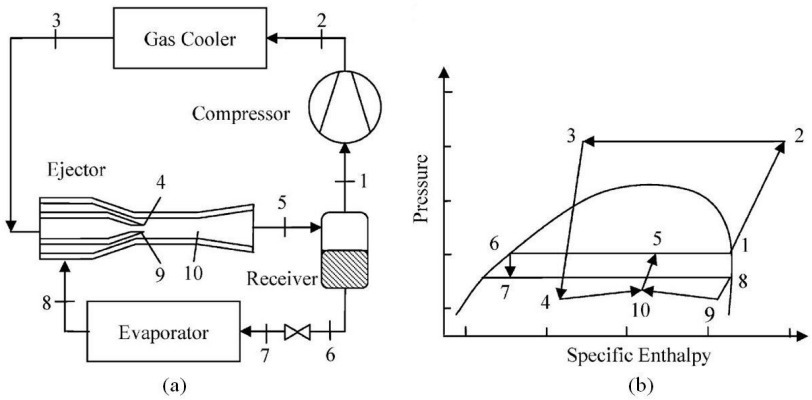

Figure 4.2 Transcritical CO2 heat pump cycle with ejector: (a) system schematic and (b) cycle p-h diagram (Sarkar, 2008)

Assuming the pressure before the inlet of the constant area section is p_b and the entrainment ratio is μ, the following equations can be identified for the ejector (Fig. 4.3).

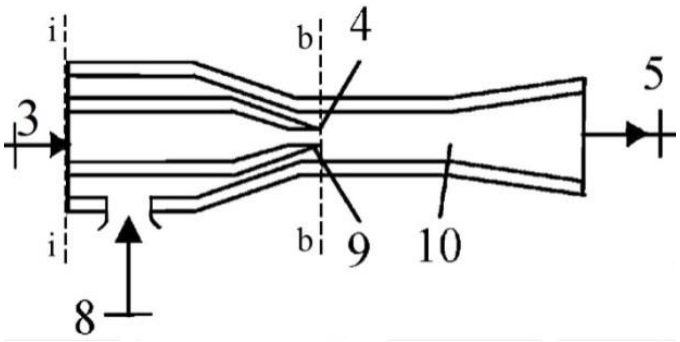

Figure 4.3 Enlarged view of the ejector (Austin & Sumathy, 2011)

The pressure of the motive stream p_3 drops to $p_b$in an isentropic process before it enters the mixing section (section b-b in Fig. 4.3). Hence,

$$s_{mb,is} = s_{mi} \tag{4.3}$$

Using equation of state the corresponding enthalpy of the motive stream can be determined.

$$h_{mb,is} = f(s_{mb,is}, p_b) \tag{4.4}$$

The actual enthalpy of the motive stream at the inlet of the content area mixing section pf the ejector can be found by using the definition of expansion efficiency.

$$\eta_m = \frac{h_{mi} - h_{mb}}{h_{mi} - h_{mb,is}} \tag{4.5}$$

Applying conservation of energy across this expansion process, the velocity of the motive stream can be found.

$$u_{mb} = \sqrt{2(h_{mi} - h_{mb})} \tag{4.6}$$

The specific volume of the motive stream at the inlet section b-b can be found using property relationship.

$$v_{mb} = f(h_{mb}, p_b) \tag{4.7}$$

The area occupied by the motive stream at section b-b per unit total ejector flow rate can be found using conservation of mass.

$$a_{mb} = \frac{v_{mb}}{u_{mb}(1 + \mu)} \tag{4.8}$$

Now, correlating the equations with state point on the p-h diagram gives –

$$\left\{ \begin{array}{c} s_{mi} = s_3 \\ h_{mi} = h_3 \\ h_{mb} = h_4 \\ u_{mb} = u_4 \\ v_{mb} = v_4 \\ a_{mb} = a_4 \end{array} \right\} \tag{4.9}$$

An analogous approach can be adopted to find the properties of the suction stream where it expands from pressure p_8 to p_b at the section b-b. Thus using the same arguments as in Eqs. 4.3 to Eqs. 4.9, the following equations can be derived.

$$s_{sb,is} = s_{si} \tag{4.10}$$

$$h_{sb,is} = f(s_{sb,is}, p_b) \tag{4.11}$$

$$\eta_s = \frac{h_{si} - h_{sb}}{h_{si} - h_{sb,is}} \tag{4.12}$$

$$u_{sb} = \sqrt{2(h_{si} - h_{sb})} \tag{4.13}$$

$$v_{sb} = f(h_{sb}, p_b) \tag{4.14}$$

$$a_{sb} = \frac{v_{sb}}{u_{sb}} \frac{\mu}{(1+\mu)} \tag{4.15}$$

$$\left\{ \begin{array}{c} s_{si} = s_8 \\ h_{si} = h_8 \\ h_{sb} = h_9 \\ u_{sb} = u_9 \\ v_{sb} = v_9 \\ a_{sb} = a_9 \end{array} \right\} \tag{4.16}$$

Applying mass, momentum and energy equation to mixing section, following equations can be derived where u_{10}, p_{10}, and h_{10} are missing velocity, pressure , and enthalpy respectively –

$$u_{mix} = u_{10} = \frac{(u_4 + \mu u_9)}{(1+\mu)} \tag{4.17}$$

$$p_{10}(a_4 + a_9) + u_{10} = p_9(a_4 + a_9) + \frac{u_4}{(1+\mu)} + \frac{\mu u_9}{(1+\mu)} \tag{4.18}$$

$$h_{10} + \frac{u_{10}^2}{2} = \frac{1}{1+\mu}\left(h_4 + \frac{u_4^2}{2}\right) + \frac{\mu}{1+\mu}\left(h_9 + \frac{u_9^2}{2}\right) \tag{4.19}$$

And for the diffuser section energy balance is given by –

$$h_5 = h_{10} + \frac{u_{10}^2}{2} \tag{4.20}$$

The overall energy balance in the ejector in given by –

$$(1+\mu)h_5 = h_3 + \mu h_8 \tag{4.21}$$

Vapor quality at the exit of the diffuser of ejector is expressed as –

$$x_5 = f(p_5, h_5) = \frac{1}{(1+\mu)} \tag{4.22}$$

Saturated liquid from separator is throttled to evaporator through expansion valve in an isentropic process yielding –

$$h_6 = h_7 \tag{4.23}$$

For the cycle the compressor work and heating capacity are in given by –

$$\dot{W}_c = \frac{1}{1+\mu}(h_2 - h_1)\dot{m}_{tot} \tag{4.24}$$

$$\dot{Q}_{gc} = \frac{1}{1+\mu}(h_2 - h_3)\dot{m}_{tot} \tag{4.25}$$

And the cooling capacity of the ejector cycle is given by –

$$\dot{Q}_{ev} = \frac{\mu}{1+\mu}(h_8 - h_6)\dot{m}_{tot} \tag{4.26}$$

In Eqs 4.22 to 4.24, $\dot{m}_{tot}$ is the total mass flow rate through the ejector. The relation among total mass flow rate, entrainment ratio, suction mass flow rate and motive mass flow rate are given by the following equations –

$$\left\{\begin{array}{c} \dot{m}_{tot} = \dot{m}_m + \dot{m}_s \\ \mu = \dfrac{\dot{m}_s}{\dot{m}_m} \\ \dot{m}_m = \dfrac{\dot{m}_{tot}}{1+\mu} \\ \dot{m}_s = \dfrac{\mu\, \dot{m}_{tot}}{1+\mu} \end{array}\right\} \tag{4.27}$$

The coefficient of performance (COP) both for cooling and heating are given by –

$$\left\{\begin{array}{l} COP_{cooling} = \dfrac{\dot{Q}_{ev}}{\dot{W}_c} \\ COP_{heating} = \dfrac{\dot{Q}_{gc}}{\dot{W}_c} \end{array}\right\} \tag{4.28}$$

4.1.3 Ejector Model in Modelica TIL Package

In TIL package the ejector model is defined by ejector efficiency. The ejector model contains a black box containing a compressor and a turbine mounted on the same shaft. According to the model the motive stream with as mass flow rate $\dot{m}_m$ expands in the turbine from supercritical pressure p_4 to intermediate pressure p_{im}. The expansion energy obtained is used to compress the suction stream that flows with the mass flow rate $\dot{m}_s$ from pressure p_{12} (evaporating pressure) to intermediate pressure p_{im}. Fig. 4.4 shows both the black box model and associated processes in p-h diagram – solid lines for ideal processes and dashed lines for real process.

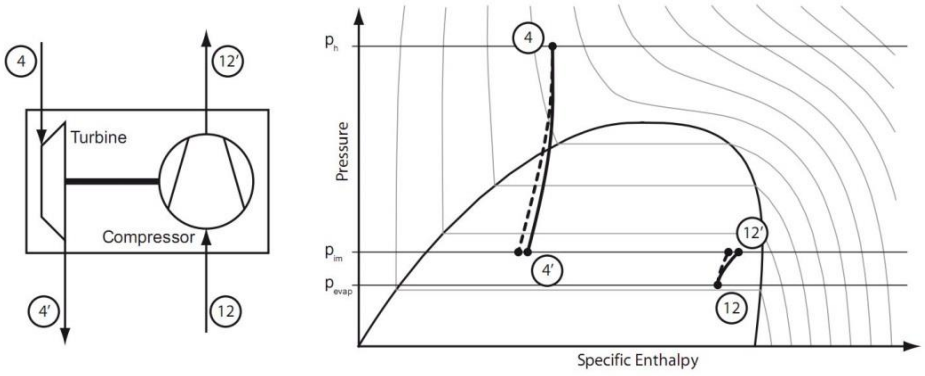

Figure 4.4 Schematic diagram of black box ejector model and corresponding p-h diagram (Richter, 2008).

The isentropic efficiencies of the compressor and the turbine can is calculated as follows –

$$\eta_{comp} = \frac{h'_{12,is} - h_{12}}{h'_{12} - h_{12}} \tag{4.29}$$

$$\eta_t = \frac{h_4 - h'_4}{h_4 - h'_{4,is}} \tag{4.30}$$

The ejector efficiency η_e is defined as the product of the two single component efficiencies and can be computed from

$$\eta_e = \eta_{copm}\eta_t = \frac{h'_{12,is} - h_{12}}{h'_{12} - h_{12}} \ \frac{h_4 - h'_4}{h_4 - h'_{4,is}} \tag{4.31}$$

The entrainment ratio can be found by the energy balance of the ejector

$$\mu = \frac{\dot{m}_s}{\dot{m}_m} = \frac{h_4 - h'_4}{h'_{12} - h_{12}} \tag{4.32}$$

Together Eqs. 4.28 and Eqs. 4.29 give the following equation for the ejector efficiency as

$$\eta_e = \frac{\dot{m}_s}{\dot{m}_m} \ \frac{h'_{12,is} - h_{12}}{h_4 - h'_{4,is}} \tag{4.33}$$

From Fig. 4.4 illustrate that the enthalpy differences in the definition of the ejector efficiency are strongly influenced by the pressure differences between high and intermediate pressure and between evaporation and intermediate pressure. The higher the pressure raise within the ejector and the higher is the suction mass flow rate, the higher the ejector efficiency.

The second parameter that influences the performance of the ejector is the shape of the primary nozzle where the motive steam is accelerated to high speed by the expense of gas cooler high pressure. The most important geometrical parameter that affects the mass flow rate through the nozzle is its smallest flow area A_0(Fig. 4.5). It is important to note that the effective flow area A_{eff} is smaller than the geometrically smallest flow area A_0.

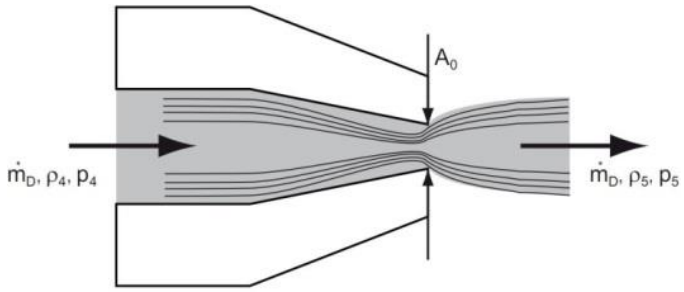

Figure 4.5 Schematic sketch of flow through a nozzle (Richter, 2008)

The mass flow rate through the nozzle is given by the following equation –

$$\dot{m}_m = A_{eff}\sqrt{2\rho_4(p_h - p_5)} \tag{4.34}$$

where, p_5 is the mixing pressure. The relation between effective flow A_{eff} area and geometric flow area is the following –

$$A_{eff} = \psi\varepsilon A_0 \tag{4.35}$$

where, the flow coefficient ψ accounts for the effects of flow contraction whereas the expansion coefficient ε takes compressibility effects into account.

In the development of the TIL package model for ejector, experiments had been conducted to measure the ejector efficiency η_e together with the value of ψ and ε. In their report it is mentioned that a major research activity has been undertaken to develop better and reliable model for the ejector as previous experiments showed low efficiency of the ejector. (Richter, 2008)

4.2 Experimental Investigation on Ejectors

The ejector model represented in section 4.1.2 considers only momentum and energy balance for the process occurring inside the ejector. However, the analysis of ejectors remains incomplete without the consideration of mass transfer that is necessary for analyzing the metastable conditions occurring during the phase transitions, which is particularly important for precise evaluation of the critical mass flow rate of the motive fluid for a given geometry of the motive nozzle. Researches have been conducted for the last two decades to develop computational codes capable of assessing the key features of the two-phase ejector performance, i.e., entrainment and pressure ratios along with the profiles of pressure, velocity

and density. Banasiak and Hafner (2011) presented a one-dimensional ejector model for CO_2 that uses a combination of several approaches adopted previously by other researchers such as Delayed Equilibrium Model supplied with the Homogeneous Nucleation Theory for the purpose of the metastable states analysis for a transcritical flow with delayed flashing over the motive nozzle. The developed model was validated based on the experiments performed at SINTEF Energi Laboratory for a typical range of operating conditions. Figure 4.6 shows the geometry on which the tests were performed.

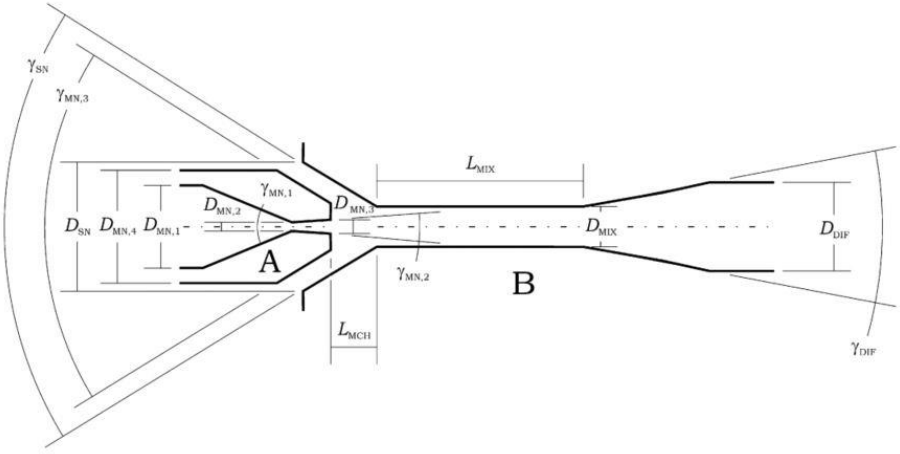

Figure 4.6 Basic geometry of the ejector used in experiment conducted by Banasiak and Hafner (Banasiak and Hafner, 2011)

An experimental and numerical investigation of the performance of ejector CO_2 heat pump cycle for different two-phase ejector geometry was carried out by Banasiak, Hafner, and Andresen (2012). The geometry of the ejector used in the experiment is similar to that of Fig. 4.6. Operating condition during experiment are the following –

- Gas cooler pressure range : 80 x 10^5 Pa to 115 x 10^5 Pa
- Gas cooler outlet temperature : ~ 303.7 K or 30.5 °C
- Evaporator pressure : ~ 35.5 x 10^5 Pa
- Evaporator temperature : ~ 0.5 °C
- Superheating at the exit of evaporator : ~ 5 K

Fig 4.7 and 4.8 show the experimental results conducted by Banasiak, Hafner, and Andresen (2012). Their numerical simulation also supports the results obtained in the experiments.

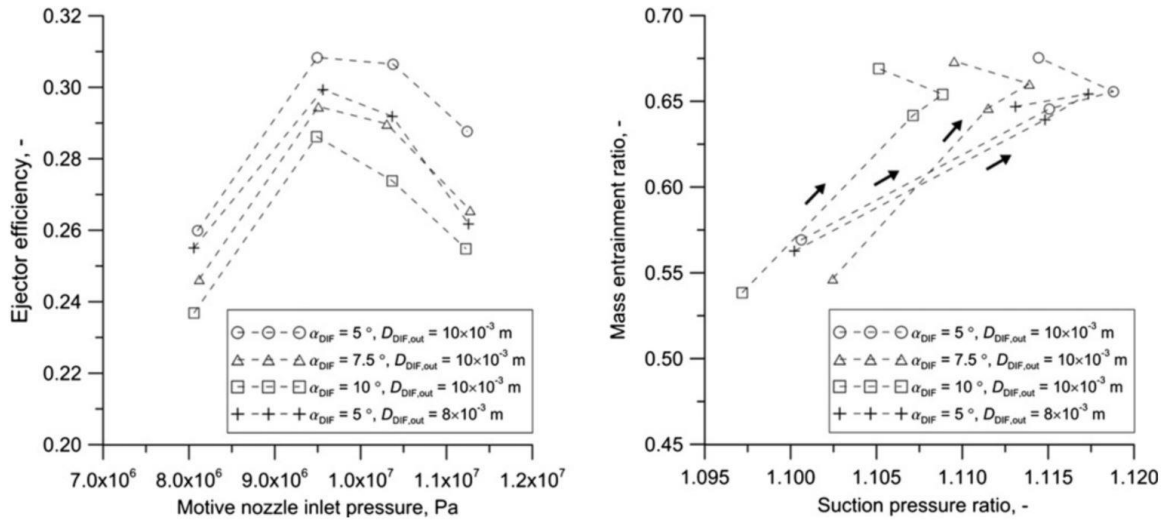

Figure 4.7 Experimental values of ejector efficiency (on the left) and the mass entrainment ration and suction pressure (on the right) for different diffuser geometries (Banasiak, Hafner, and Andresen, 2012)

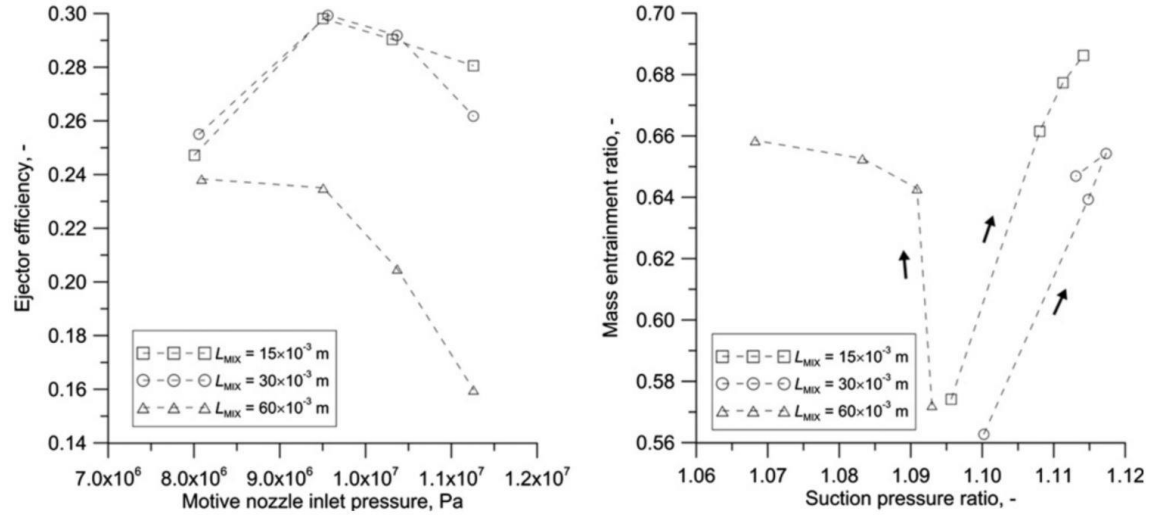

Figure 4.8 Experimental values of ejector efficiency (on the left) and the mass entrainment ration and suction pressure (on the right) for different mixer lengths (Banasiak, Hafner, and Andresen, 2012)

Based on their experiment the 5° divergence angle proved to yield the highest values of the ejector efficiency among all geometry options examined, and the best mixer length was equal to 30 x 10^{-3} m together with best mixing section diameter 3 x 10^{-3} m.

4.2.1 Utilization of the Experimental Results

In this thesis the experimental results found by Banasiak et al. (2012) will be used for the steady state ejector cycle calculation, and the ejector geometry would be the best configuration suggested by the authors –

- Divergence angle : 5°
- Mixing section length : 30 x 10^{-3} m
- Mixing section diameter : 3 x 10^{-3} m

Table 4.1 shows the experimental results for the particular geometry of the ejector.

Table 4-1 Experimental results for the particular geometry of the ejector

Gas cooler outlet pressure, Pgc [bar]	Entrainment ratio [-]	Suction pressure ratio [-]	Ejector efficiency
81.2	0.569	1.10063	0.26
95	0.64375	1.115	0.30875
103.75	0.65625	1.11875	0.30625
115	0.675	1.11438	0.2875

Fig 4.9, 4.10, and 1.11 show the relations between gas cooler outlet pressure with entrainment ration, suction pressure ration and ejector efficiency respectively. With increase in gas cooler outlet pressure entrainment ratio also increases. However, the rate of increase is less compared to pressure interval 80 bar to 95 bar. On the other hand, suction pressure ration shows an increase in value with gas cooler outlet pressure till pressure reaches 103 bar and decreases onwards with increase in pressure. Ejector efficiency shows it highest vale around 95 bar.

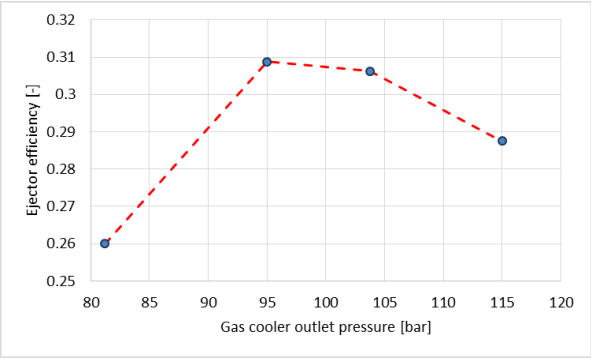

Figure 4.9 Relation between ejecor efficiency and gas cooler pressure

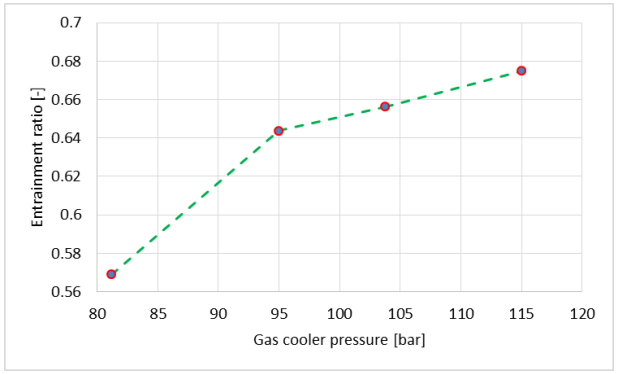

Figure 4.10 Relation between entrainment ratio and gas cooler pressure

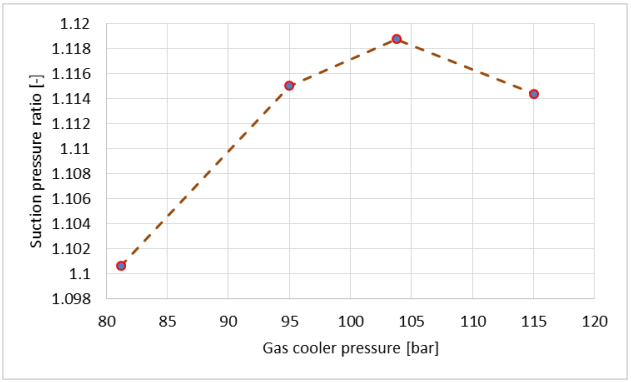

Figure 4.11 Relation between suction pressure ratio and gas cooler pressure

In order to utilize these experimental data in steady state caiculation, following piecewise liniar relationship can be derived both for entrainment ratio and suction pressure ratio.

$$Entrainment\ ratio\ , \mu = \begin{cases} 5.417 \times 10^{-3} p_{gc} + 0.1292 \ ; \ 81.2 \leq p_{gc} < 95 \\ 1.4286 \times 10^{-3} p_{gc} + 0.5080 \ ; \ 95 \leq p_{gc} < 103.75 \\ 1.667 \times 10^{-3} p_{gc} + 0.4833 \ ; \ 103.75 \leq p_{gc} < 115 \end{cases} \quad (4.36)$$

$$Suction\ pressure\ ratio\ or\ Pressure\ lift\ ratio, PLR = \begin{cases} 1.0417 \times 10^{-3} p_{gc} + 1.01604 \ ; \ 81.2 \leq p_{gc} < 95 \\ 4.2857 \times 10^{-3} p_{gc} + 1.07429 \ ; \ 95 \leq p_{gc} < 103.75 \\ -3.889 \times 10^{-4} p_{gc} + 1.1591 \ ; 103.75 \leq p_{gc} < 115 \end{cases} \quad (4.37)$$

5 Case Study and Solution Approach

This chapter contains the description of the systems considered for study along with their respective equations and boundary conditions. The first system considered is the conventional CO_2 TRC cycle with expansion valve, suction gas heat exchanger, air cooled gas cooler, and a gas cooler coupled to borehole heat exchanger. The other system comprises of an ejector instead of expansion vale without suction gas heat exchanger when other components remain the same.

5.1 Design Concept and constrains

In summer dominating countries, the ambient air temperature could reach above 40 °C during hot summer days. A CO_2 TRC building cooling system rejecting heat to ambient air in such a climate would face a minimum temperature up to which it can reject heat before the working fluid is throttled down to low pressure in order to provide cooling. Furthermore, in order to have effective heat transfer between the working fluid and ambient air, a temperature difference must be provided which would result in even a higher temperature limit.

CO_2 T-h diagram can be used to visualize this constraint posed by high ambient temperature (Fig. 5.1). Let us consider the maximum air temperature 40 °C and temperature difference for effective heat transfer 5 °C. Consequently minimum temperature up to which supercritical CO_2 can be cooled is 45 °C. Theses temperatures are shown in green and yellow lines respectively in Fig. 5.1. Now, if we consider a conventional cycle C'-E-D_9-C where the high pressure is 9 MPa, due to the constraint of T = 45 °C the cycle will have very low refrigerating effect (length C'E) consequently poor cooling COP. However, for the given constraint if the pressure is increased to 10 MPa (cycle B'-E-D_{10}-B), the refrigerating effect will increase resulting in a higher cooling COP. Although further increase in pressure will also increase the refrigeration effect, systems with very high pressure are infeasible and uneconomic. Apart from these, the diagram shows something very significant that is if the gas cooler outlet temperature could have been lowered beyond T = 45 °C to less than 30 °C, the refrigeration effect would increase significantly even at a low pressure.

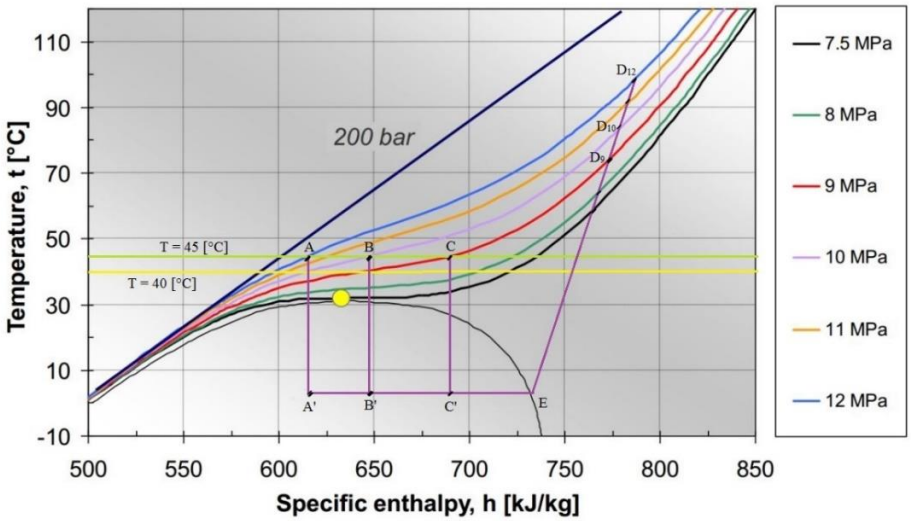

Figure 5.1 T-h diagram to illustrate the ambient air temperature constraint on CO_2 transcricital cycle

It is evident from the above discussion that in order to have better cooling performance the system should have an optimum operating pressure and low gas cooler outlet temperature. This can be achieved by introducing another gas cooler into the system that is connected to a borehole heat exchanger where the soil functions as a heat sink whose temperature is relatively low and stable compared to ambient air temperature. Thus, it is possible to lower the outlet temperature of the gas cooler side equal or below to 30 °C for an optimum pressure. However, the amount of heat ejection to the borehole depends on the thermal properties of the soil and the length of the borehole. Furthermore, the length of the borehole is an economic decision, and it is necessary to investigate overall system configuration and performance before implementing such systems. This thesis investigates CO_2 TRC systems that operates with two gas coolers – one rejecting heat to ambient air and another to the soli through a borehole heat exchanger for a constraint posed by the maximum ambient temperature. The system configurations considered (for steady state calculation) are –

1. Hybrid system with expansion valve (HS1): the main components are evaporator, low pressure receiver, suction gas heat exchanger, compressor, air cooled gas cooler, gas cooler coupled to borehole heat exchanger, and expansion valve.
2. Hybrid system with ejector (HS2): the main components are evaporator, low pressure side expansion valve, liquid separator, compressor, air cooled gas cooler, gas cooler coupled to borehole heat exchanger, and ejector.

Before performing simulation in Modelica, it is necessary to perform steady state calculation of the system configurations mentioned above. In further discussion system with expansion valve and system with ejector will be referred as HS1 and HS2 respectively. For both of the systems, some assumptions were made during calculation, namely –

- No pressure drop in the pipes
- No heat loss form the heat exchangers
- No heat loss from the compressor

5.1.1 Boundary condition for HS1

Table 5.1 summarizes the boundary conditions for HS1 steady state calculation.

Table 5-1 Boundary conditions for HS1

Cooling load	10	[kW]
Evaporating Temperature	0	[°C]
Evaporating Pressure	34.85	[bar]
Gas cooler pressure	100	[bar]
Superheating before compressor inlet	5	[°C]
Compressor isentropic efficiency	0.8	[-]
Compressor volumetric efficiency	0.8	[-]
Maximum air temperature	40	[°C]
Temperature difference at air cooled gas cooler outlet	5	[°C]
Outlet temperature of the second gas cooler	30	[°C]
Heat transfer per unit depth of soil	40	[W/m]

5.1.2 Boundary condition for HS2

Table 5.2 summarizes the boundary conditions for HS2 steady state calculation

Table 5-2 Boundary conditions for HS2

Cooling load	10	[kW]
Evaporating Temperature	0	[°C]
Superheating at evaporator exit (ejector inlet condition)	5	[°C]
Evaporating Pressure	34.85	[bar]
Gas cooler pressure	100	[bar]
Superheating before compressor inlet	No superheating	[-]
Compressor isentropic efficiency	0.8	[-]
Compressor volumetric efficiency	0.8	[-]
Maximum air temperature	40	[°C]
Temperature difference at air cooled gas cooler outlet	5	[°C]
Outlet temperature of the second gas cooler	30	[°C]
Heat transfer per unit depth of soil	40	[W/m]

5.2 Governing equations for steady state calculation

5.2.1 Mathematical model for HS1

Fig 5.2 and 5.3 show the p-h and system's schematic diagram for HS1 respectively. With afore mentioned boundary conditions the following governing equations can be written for this system. This mode was implemented in RnLib .

5.2.1.1 Evaporator

For a given evaporator load –

$$\dot{Q}_{evp} = \dot{m}_r(h_a - h_4) \tag{5.1}$$

where, $\dot{Q}_{evp}$ and $\dot{m}_r$ represent evaporate duty and refrigerant mass flow rate. Enthalpy is represented by h and subscript with it represents the point on p-h diagram.

5.2.1.2 Suction gas heat exchanger

Assuming the effectiveness of the suction has heat exchanger $\varepsilon = 1$, the following equations can be written –

$$\begin{cases} h_3 - h_b = h_1 - h_a \\ h_1 = function\left(p_{evp}, T_1 = T_{evp} + 5°C\right) \\ Saturated\ gas\ enthalpy, h_a = function(p_{evp}\ or\ T_{evp}) \end{cases} \quad (5.2)$$

5.2.1.3 Compressor

$$\begin{cases} \dot{W}_{com} = \dot{m}_r(h_2 - h_1) \\ h_2 = h_1 + \dfrac{h_{2s} - h_1}{\eta_s} \end{cases} \quad (5.3)$$

where, $\dot{W}_{com}$ and η_s represent compressor work and its isentropic efficiency respectively.

5.2.1.4 Air cooled gas cooler

$$\begin{cases} \dot{Q}_{gc,air} = \dot{m}_r(h_2 - h_c) \\ h_c = function(p_{gc}, T_c = 45°C) \end{cases} \quad (5.4)$$

where, $\dot{Q}_{gc,air}$ represents the amount of heat that is rejected to air before supercritical CO_2 rehashes 45 °C at the given gas cooler pressure.

5.2.1.5 Gas cooler connected to borehole heat exchanger

$$\begin{cases} \dot{Q}_{gc,bh} = \dot{m}_r(h_a - h_4) \\ h_3 = function\left(p_{gc}, T_3 = 30°C\right) \end{cases} \quad (5.5)$$

5.2.1.6 Expansion valve

Isenthalpic process takes place in the expansion valve, thus –

$$h_b = h_4 \quad (5.6)$$

The coefficient of performances are given by –

$$\left\{\begin{array}{c} COP_{cooling} = \dfrac{\dot{Q}_{evp}}{\dot{W}_{com}} \\ COP_{heating} = \dfrac{\dot{Q}_{gc,air} + \dot{Q}_{gc,bh}}{\dot{W}_{com}} \end{array}\right\} \tag{5.7}$$

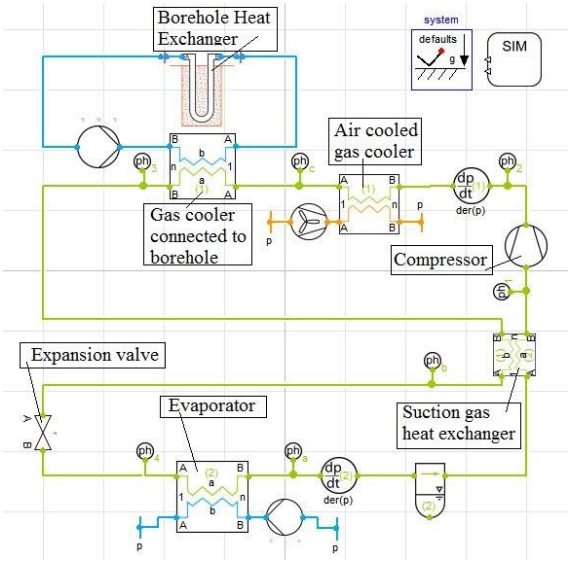

Figure 5.2 Schematic diagram of HS1

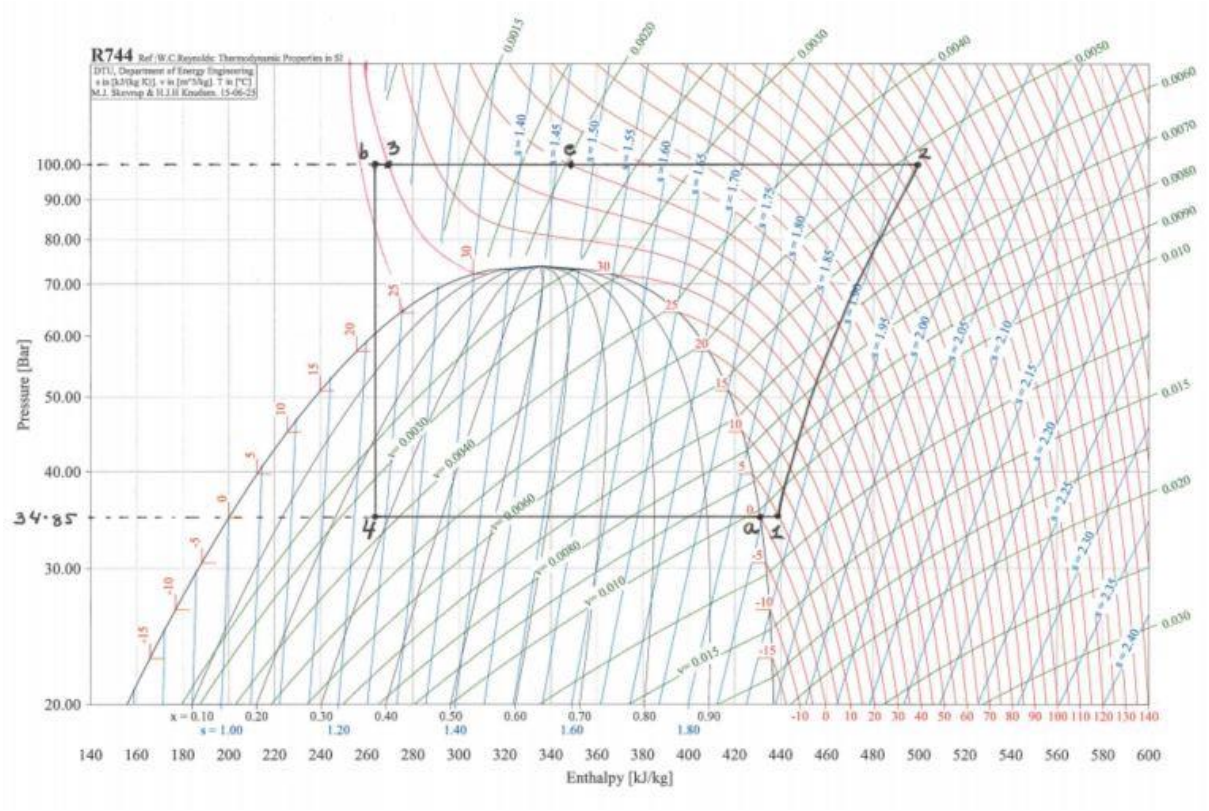

Figure 5.3 p-h diagram for HS1

5.2.2 Mathematical model for HS2

The inadequacy of the model presented in section 4.1.2 can be overcome by using experimental correlation developed in section 4.2.1 for prediction of entrainment ration and suction pressure ration when gas cooler pressure is given. As the boundary condition for HS2 matches the experimental condition by Banasiak et al. (2012), there following steady state calculation can be performed for CO_2 TRC ejector cycle. System calculation was carried out both in RnLib and EES (Engineering Equation Solver).

5.2.2.1 Ejector

The ejector entrainment ratio and suction pressure ratio are connected to gas cooler pressure by –

$$Entrainment\ ratio\ , \mu = \begin{cases} 5.417 \times 10^{-3} p_{gc} + 0.1292 \ ; \ 81.2 \leq p_{gc} < 95 \\ 1.4286 \times 10^{-3} p_{gc} + 0.5080 \ ; \ 95 \leq p_{gc} < 103.75 \\ 1.667 \times 10^{-3} p_{gc} + 0.4833 \ ; \ 103.75 \leq p_{gc} < 115 \end{cases} \quad (5.8)$$

$$Suction\ pressure\ ratio\ or\ Pressure\ lift\ ratio, PLR = \begin{cases} 1.0417 \times 10^{-3} p_{gc} + 1.01604 \ ; \ 81.2 \leq p_{gc} < 95 \\ 4.2857 \times 10^{-3} p_{gc} + 1.07429 \ ; \ 95 \leq p_{gc} < 103.75 \\ -3.889 \times 10^{-4} p_{gc} + 1.1591 \ ; 103.75 \leq p_{gc} < 115 \end{cases} \quad (5.9)$$

The relation for entrainment ration and mass flowrates is given by –

$$\left\{ \begin{array}{c} \dot{m}_{tot} = \dot{m}_m + \dot{m}_s \\ \mu = \dfrac{\dot{m}_s}{\dot{m}_m} \\ \dot{m}_m = \dfrac{\dot{m}_{tot}}{1+\mu} \\ \dot{m}_s = \dfrac{\mu\, \dot{m}_{tot}}{1+\mu} \end{array} \right\} \quad (5.10)$$

Ejector efficiency is given by –

$$\eta_e = \mu \frac{h_b - h_6}{h_4 - h_a} \quad (5.11)$$

Ejector energy balance gives –

$$(1+\mu) h_7 = h_3 + \mu h_6 \quad (5.12)$$

Evaporator

For a given evaporator load –

$$\begin{cases} \dot{Q}_{evp} = \dfrac{\mu}{1+\mu}(h_6 - h_5)\dot{m}_{tot} \\ h_6 = function(p_{evp}, T_6 = T_{evp} + 5°C) \end{cases} \tag{5.13}$$

5.2.2.2 Expansion valve

For isenthalpic expansion process –

$$h_4 = h_5 \tag{5.14}$$

5.2.2.3 Liquid separator

Energy and mass balance for the liquid separator are given by –

$$\begin{cases} (1+\mu)h_7 = h_1 + \mu h_4 \\ (1+\mu)x_7 = 1 \\ x_7 = function(p_7, h_7) \end{cases} \tag{5.15}$$

where,

$$p_7 = p_4 = p_1 = p_{evp} \times PLR \tag{5.16}$$

5.2.2.4 Compressor

$$\begin{cases} \dot{W}_{com} = \dot{m}_r(h_2 - h_1) \\ h_2 = h_1 + \dfrac{h_{2s} - h_1}{\eta_s} \end{cases} \tag{5.17}$$

where, $\dot{W}_{com}$ and η_s represent compressor work and its isentropic efficiency respectively

5.2.2.5 Air cooler gas cooler

$$\begin{cases} \dot{Q}_{gc,air} = \dot{m}_r(h_2 - h_c) \\ h_c = function(p_{gc}, T_c = 45°C) \end{cases} \tag{5.18}$$

where, $\dot{Q}_{gc,air}$ represents the amount of heat that is rejected to air before supercritical CO_2 rehashes 45 °C at the given gas cooler pressure.

5.2.2.6 Gas cooler connected to borehole heat exchanger

$$\begin{cases} \dot{Q}_{gc,bh} = \dot{m}_r(h_a - h_4) \\ h_3 = function(p_{gc}, T_3 = 30°C) \end{cases} \tag{5.19}$$

The coefficient of performances are given by –

$$\left\{ \begin{array}{c} COP_{cooling} = \dfrac{\dot{Q}_{evp}}{\dot{W}_{com}} \\ COP_{heating} = \dfrac{\dot{Q}_{gc,air} + \dot{Q}_{gc,bh}}{\dot{W}_{com}} \end{array} \right\} \tag{5.20}$$

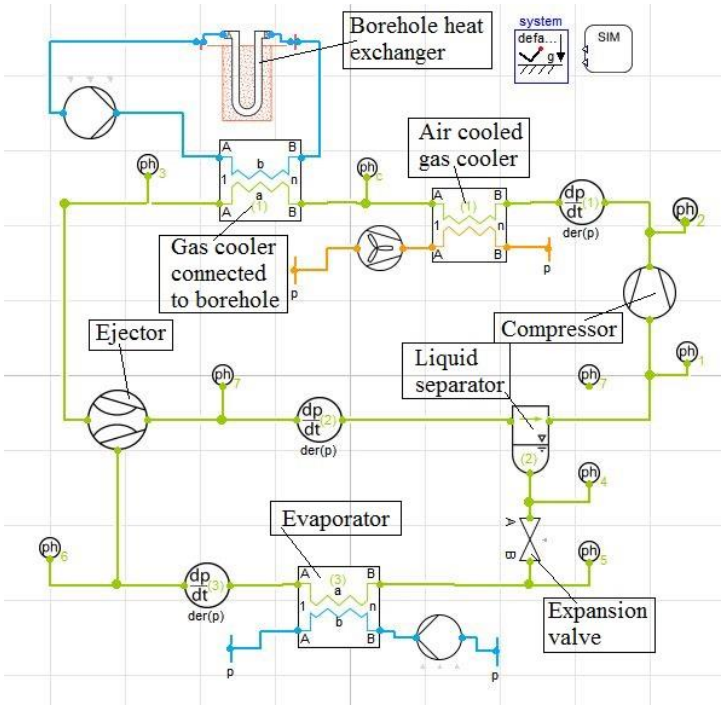

Figure 5.4 Schematic diagram of HS2

In Fig 5.4 the component arrangement for HS2 is shown schematically. At this point it is important to mention that the actual process taking place inside the ejector cannot be represented in a p-h diagram. In Fig 5.5 this processes are shown in dotted lines. The line joining point 3 and 9 represents the process taking place inside the motive nozzle, point 10 represents the mixing of the two streams, and line 10 to 7 represents the pressure increase in the diffuser section.

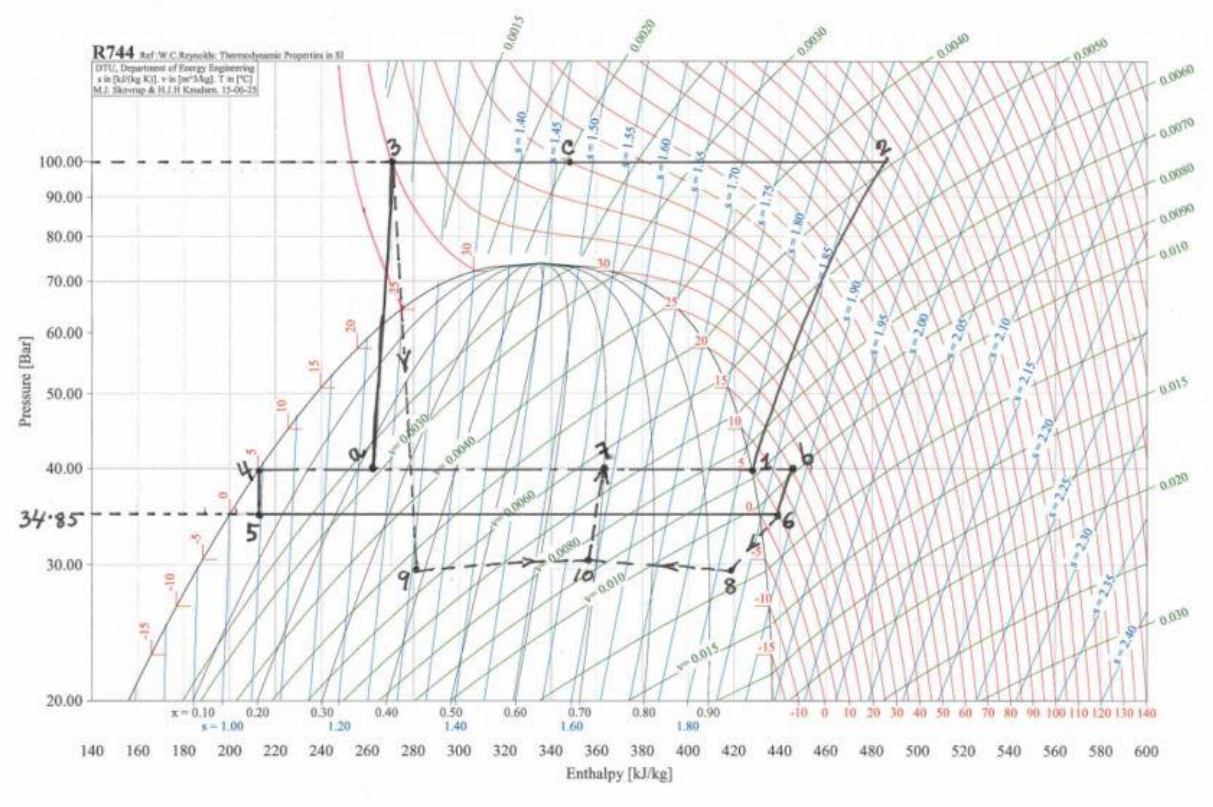

Figure 5.5 p-h diagram of HS2 (CO2 transcritical cycle with ejector)

5.3 Modelica simulation initialization

Before conducting simulation in Modelica (Dymola platform), it is necessary to size the components that would be used during simulation. The results found from the steady state calculation of HS1 and HS2 were used during simulation initialization. Some of the basic calculation was also done using RnLib.

6 Results and Discussion

Before discussing the results obtained, it is necessary to define the investigations that were made during the simulation. For HS1 and HS2 the keys questions investigated were –

1. Comparison of coefficient of performance (cooling) for both system configurations
2. Compression power required for each configuration
3. Load on air cooled gas cooler for constraints posed by ambient air temperature
4. For specified thermal properties of soil, required length of the borehole for both systems
5. Comparison between HS2 steady state calculation and Modelica results
6. HS2 Modelica System response with respect to ambient temperature change
7. Performance comparison for theoretical and Modelica systems

6.1 Performance comparisons of the systems

As HS1 comprises of CO_2 TRC cycle with expansion valve, in the steady state case there is only one mass flow rate in the system. A 5°C superheat before inlet of the compressor is provided to make sure that no liquid goes into the compressor as well as to decrease the work of compression. This superheating is provided by the use of a suction has heat exchanger, and the advantage of it was discussed in section 2.3.1. However, HS2 which operates on standard CO_2 cycle does not have a suction gas heat exchanger, and there are two mass flow rate in the system, namely motive mass flow and suction mass flow. At the end of the evaporator a 5°C superheat was provide to improve entrainment capacity of the motive flow. The theoretical analysis shows that the cooling performance of HS2 is on an average 8% higher than HS1 for pressure varying from 81 to 115 bar. It should be noted that the motive mass flow rate of HS2 depends on the gas cooler pressure unlike HS1 where mass flow rate is constant.

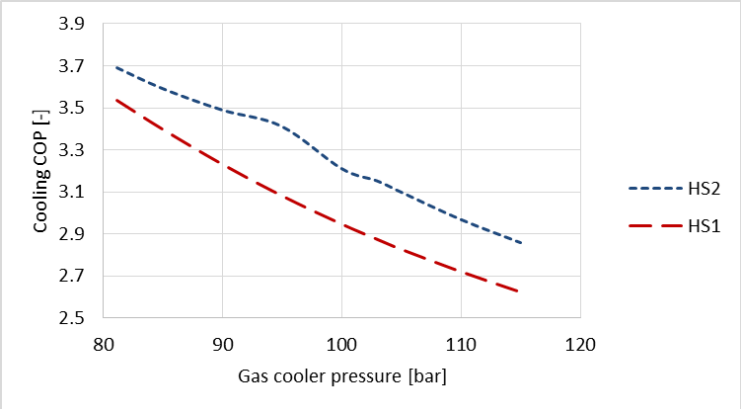

Figure 6.1 Cooling COP comparison of the system HS1 and HS2

6.2 Refigured compression power

Fig. 6.2 shows the compressor power required for both HS1 and HS2. On average the compressor power needed for ejector cycle (HS2) is 8% less than conventional expansion valve cycle (HS1) when gas cooler pressure ranges from 81 to 115 bar. This explains the COP improvement achieved by HS2 discussed in the last section. The reason behind less power consumption is that in HS2 the compressor operates for lower pressure ratio compared to HS1. Although for HS2 mass flow rate through the compressor is on average 14% higher than HS1, the pressure ratio for compressor is lowered by ejector action giving low power requirement for HS2 (Fig. 6.3).

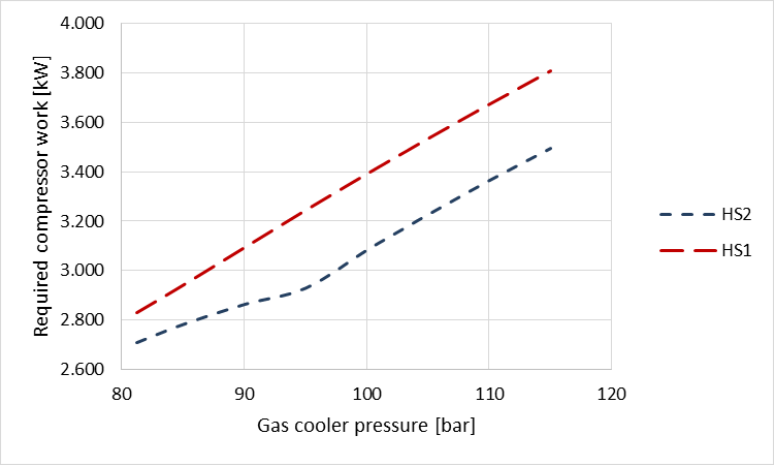

Figure 6.2 Compressor power comparison between HS1 and HS2

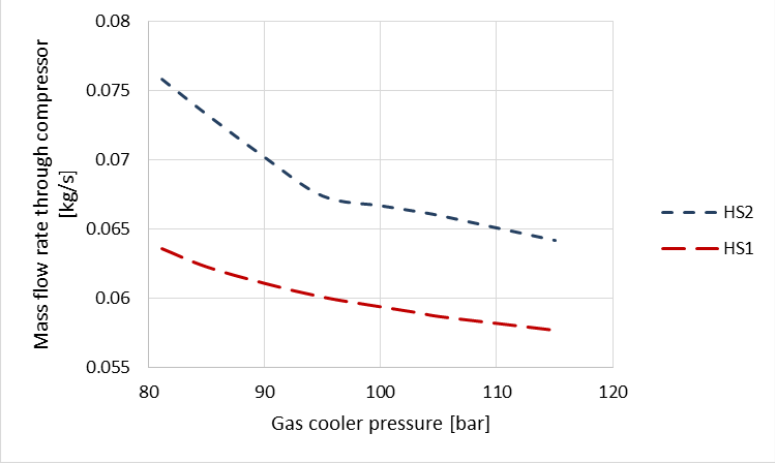

Figure 6.3 Mass flow rate through compressor and gas coolers in HS1 and HS2

6.3 Load on air cooled gas cooler

As there exits constraint from ambient air temperature, the air cooled gas coolers for both system configuration can handle certain amount of load with respect to total cooling load of 10 kW at a given gas cooler pressure. A parameter called 'Relative Cooling Load Capacity of Air Cooled Gas Cooler (RAGC)' for a given pressure can be defined as following –

$$Relative\ cooling\ load\ capacity\ of\ air\ cooled\ gas\ cooler\ (RLAGC) = \frac{\dot{Q}_{gc,air}}{\dot{Q}_{evap}} \times 100\% \quad (6.1)$$

Fig. 6.4 shows the relative comparison of RAGC for both HS1 and HS2. HS2 has less RLAGC for a given pressure due to the fact that the mass flow rate in HS2 is higher than HS1 for that gas cooler pressure. Thus, in HS2 the supercritical CO_2 reaches temperature limit (45°C in this case) faster than HS1. One consequence of this fact is for HS2 load on the second gas cooler would be higher compared to HS1, and this would lead to longer borehole length for ejector cycle.

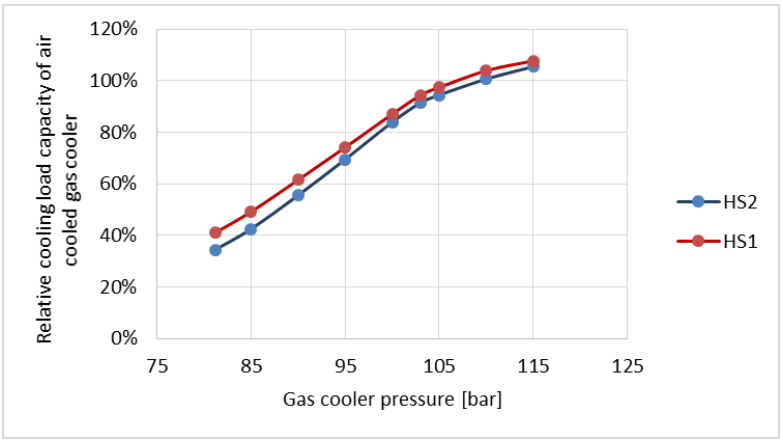

Figure 6.4 Comparison of relative load handling capacity of air cooled gas cooler for HS1 and HS2

6.4 6.4 Required length of the borehole

Fig. 6.5 shows the required borehole length for both HS1 and HS2 when heat transfer rate per unit borehole length is assumed to be 40 W/m. As mentioned earlier that for ejector cycle (HS2) the mass flow rate is higher than expansion valve cycle (HS1), the load on the borehole heat

exchanger is higher for given cooling load and gas cooler pressure. For both the systems the length required is less at high gas cooler pressure as the air cooled gas cooler has high load handling capacity (RLAGC). It should be emphasized at this point that the thermal properties of the soil would play an important role for determining the required borehole length. For a particular location experiments needs to be done to predict soil thermal behavior before implementing such systems.

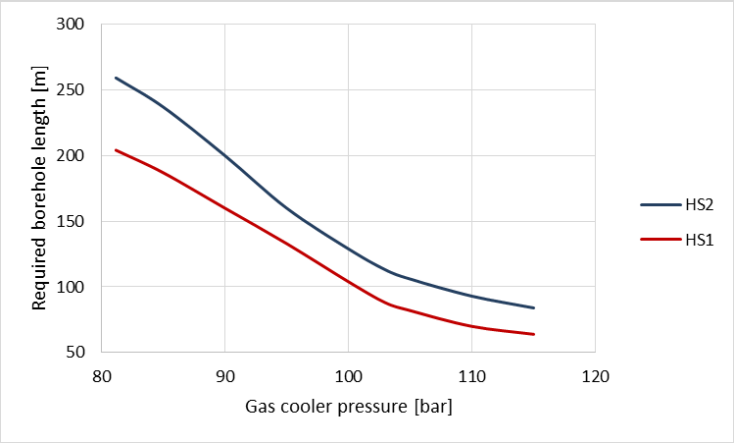

Figure 6.5 Comparison of required borehole length for HS1 an HS2

6.5 HS2 steady state calculation vs. Modelica results

In the Fig 6.6 the cooling performance for steady state HS2 and HS2 Modelica simulation are plotted against gas cooler pressure ranging from 85 to 115 bar. Though the cooing performance shows similar pattern for both of the system, the COP of HS2 Modelica is lower than the theoretical HS2 except for pressure around 100 bar. This is further explained by Fig 6.7 which shows that compressor work required for this two systems. It shows that near 100 bar the compressor work for HS2 Modelica is almost equal to the work required for theoretical HS2. For pressure higher than 100 bar, the work for HS2 Modelica remains higher than theoretical calculation. The difference in compressor work and COP may result from the fact that the ejector model used in Modelica over predicts the entrainment ratio than the experimental results that had been used for theoretical calculation (Fig. 6.8).

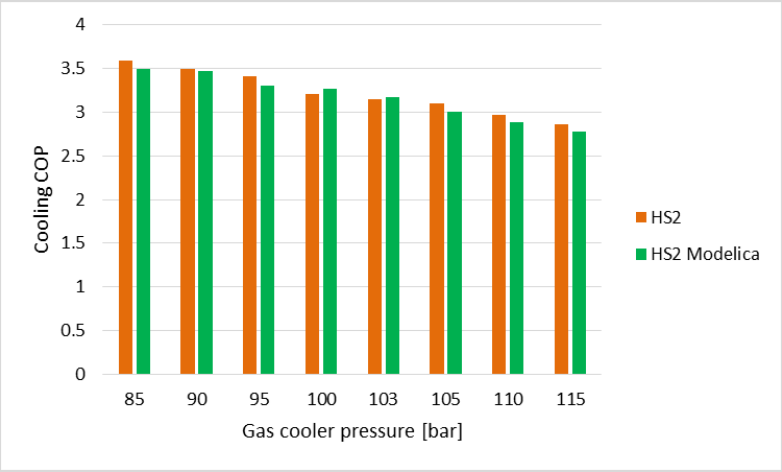

Figure 6.6 Comparison for COP of HS2 Modelica simulation and theoretical HS2

At this point it is necessary to mention that ejector model in Modelica uses three different nozzle equation, namely incompressible nozzle flow (Bernoulli equation), compressible nozzle flow (Energy balance equation), and flow correlation of Lucas. During the simulation compressible nozzle flow equation was used, and it has some shortcoming as mentioned before in section 4.2.

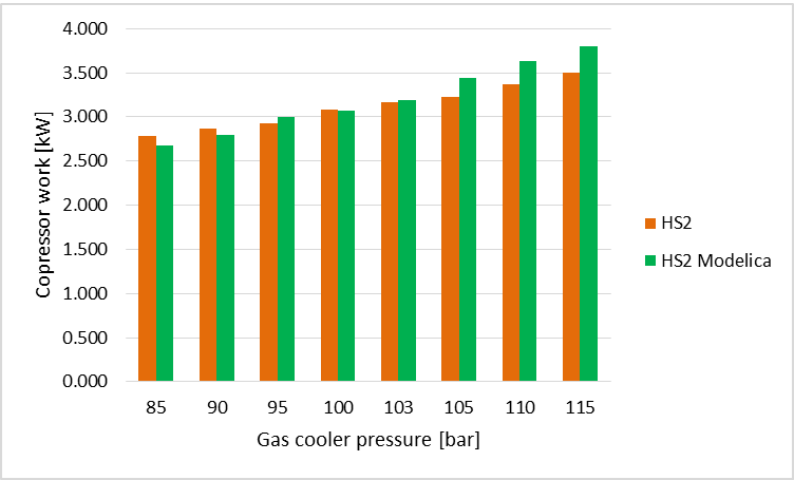

Figure 6.7 Comparison for compressor work requirement for HS2 Modelica simulation and theoretical HS2

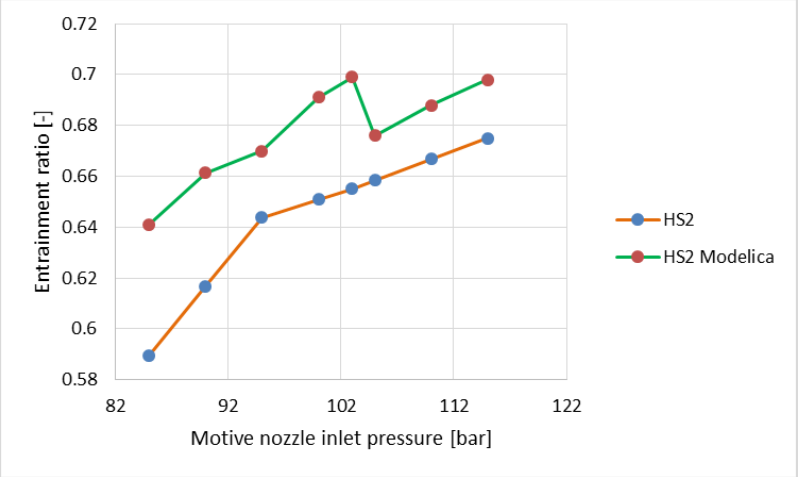

Figure 6.8 Comparison for entrainment ratio predicted by Modelica simulation (use of energy equation for nozzle) and experimental data (Banasiak et al experiment in 2012)

6.6 Temperature response of HS2 Modelica system

The variation of ambient air temperature was considered as 32 °C (305 K) to 40 °C (313 K), and it was approximated with a trapezoidal temperature variation over 14 hours period while the gas cooler side pressure was kept constant using a PI controller (Fig. 6.9). The corresponding load response of the gas coolers for a particular size and capacity are shown in Fig.6.10. During the first four hours when the ambient air temperature is constant, the loads on the gas cooler also remain constant. However, whenever the temperature begins to rise, the load on the gas cooler connected to the borehole increase and load handling capacity the air cooled gas cooler decreases. During the peak temperature period, the heat rejection capacity of the second gas cooler decrease to some extent because of the rise of soil temperature, thus the outlet temperature of CO_2 increases slightly which impacts the system COP.

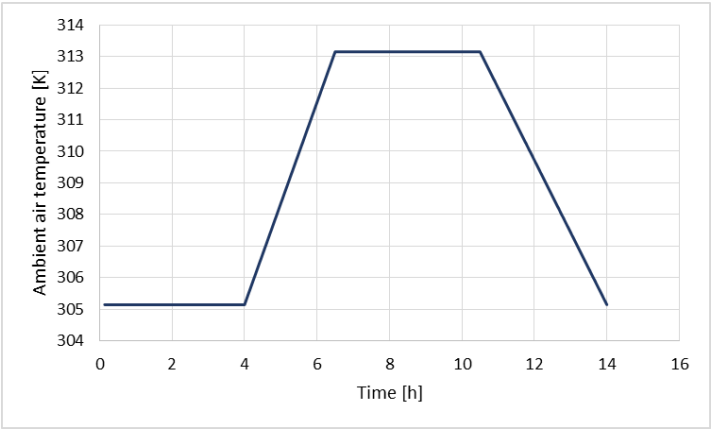

Figure 6.9 Trapezoidal temperature profile

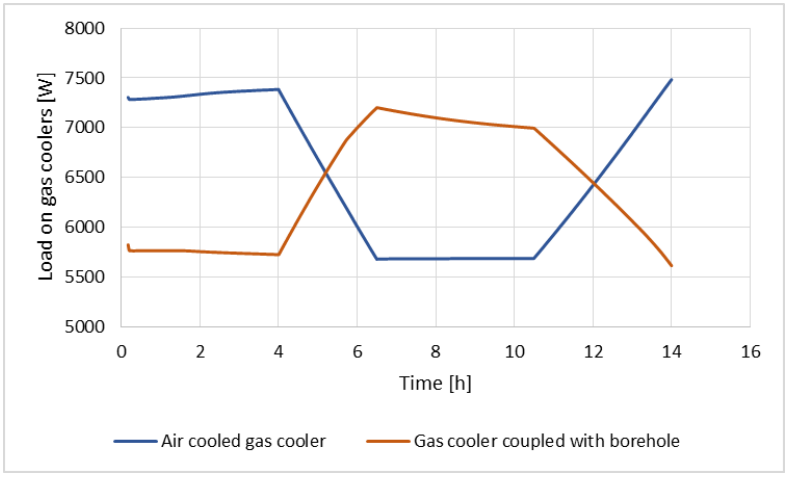

Figure 6.10 Load response of the gas coolers for a trapezoidal temperature variation of ambient air

6.7 Performance comparison of theoretical and simulated systems

Fig. 6.11 summarizes cooling COP for all the systems for particular gas cooler pressure. The common trend is that with high pressure the cooling COP decreases for all systems. In all the cases cycle with ejector shoes better perform than cycle with expansion vale and suction gas heat exchanger. With no use of suction as heat exchanger is ejector cycle an economic advantage along with performance can be achieved.

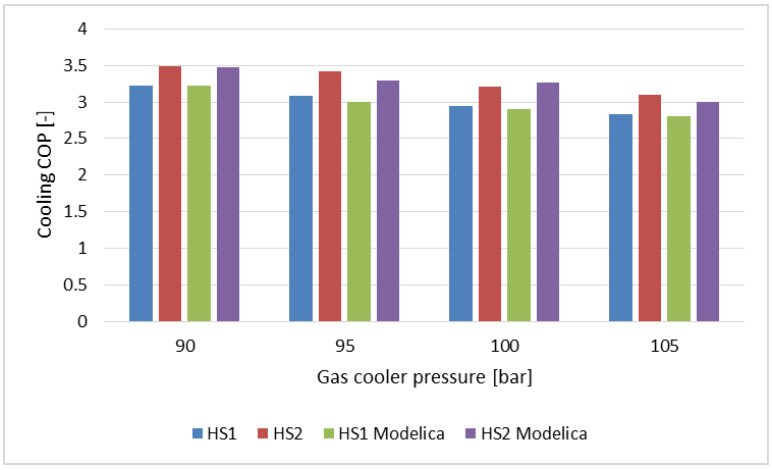

Figure 6.11 Cooling performance of theoretical and Modelica simulated systems

7 Conclusion

Based on the investigation made in this thesis the following conclusion can be drawn –

- The cooling performance of ejector cycle for ground-coupled CO_2 system is better than conventional expansion valve cycle with suction gas heat exchanger. By using an ejector expansion energy can be utilized to raise pressure of the suction stream, thus pressure ratio of the compressor decreases. This helps the system to achieve better COP. Furthermore, the cost of suction gas heat exchanger could be saved in ejector systems.
- In ejector cycle the mass flow rate through the compressor and gas cooler depend on the entrainment ration. This mass flow (motive mass flow rate) is higher than that of expansion cycle for the same cooling load. Consequently load on the gas cooler side is higher than expansion valve system. This indicates that the length of the borehole would higher for ejector system.
- The thermodynamic and fluid mechanic behavior of ejector is complex, and it is necessary to use experimental data for particular ejector geometry for system analysis.
- Ejector efficiency, entrainment ratio, and suction pressure are dependent on ejector geometry. Thus, only momentum and energy balance for correct simulation of heat pumping systems is not enough.
- In order to predict behavior of the borehole heat exchanger, experimental data is necessary for longer period of time. This behavior may vary place to place.
- For Modelica simulation proper sizing of the heat exchanger is necessary. However, the documentation for the heat exchanger lacks information. In some cases trial and error method was only method.

<u>Suggestion for Future Work</u>

- For borehole heat exchanger model an updated library should be used that matches with newer versions of Dymola. Better documentation for the mathematical model is necessary for reliable simulation.
- Better mathematical model of the ejector can be built in Modelica platform that takes mass and heat transfer in to account along with momentum and energy conservation.
- Actual weather data can be utilized for prediction of the system behavior.
- Further investigation can be made for designing control system for ejector cycle.

- Effort can be invested to model heat exchangers in Modelica that can be used in further heat pumping system simulation.

References

Agrawal, N., Bhattacharyya, S., & Sarkar, J. (2007). Optimization of two-stage transcritical carbon dioxide heat pump cycles. *International Journal of Thermal Sciences, 46*(2), 180-187. doi: DOI 10.1016/j.ijthermalsci.2006.04.011

Ahammed, M. E., Bhattacharyya, S., & Ramgopal, M. (2014). Thermodynamic design and simulation of a CO2 based transcritical vapour compression refrigeration system with an ejector. *International Journal of Refrigeration-Revue Internationale Du Froid, 45*, 177-188. doi: DOI 10.1016/j.ijiefrig.2014.06.010

ASHRAE. (2001). Atlanta: American Society of Heating, Refrigerating, and Airconditioning Engineers.

Asinari, P., Cecchinato, L., & Fornasieri, E. (2004). Effects of thermal conduction in microchannel gas coolers for carbon dioxide. *International Journal of Refrigeration-Revue Internationale Du Froid, 27*(6), 577-586. doi: DOI 10.1016/j.ijrefrig.2004.04.001

Austin, B. T., & Sumathy, K. (2011). Transcritical carbon dioxide heat pump systems: A review. *Renewable & Sustainable Energy Reviews, 15*(8), 4013-4029. doi: DOI 10.1016/j.rser.2011.07.021

Banasiak, K., & Hafner, A. (2011). 1D Computational model of a two-phase R744 ejector for expansion work recovery. *International Journal of Thermal Sciences, 50*(11), 2235-2247. doi: DOI 10.1016/j.ijthermalsci.2011.06.007

Banasiak, K., Hafner, A., & Andresen, T. (2012). Experimental and numerical investigation of the influence of the two-phase ejector geometry on the performance of the R744 heat pump. *International Journal of Refrigeration-Revue Internationale Du Froid, 35*(6), 1617-1625. doi: DOI 10.1016/j.ijrefrig.2012.04.012

Bendaoud, A., Ouzzane, M., Aidoun, Z., & Galanis, N. (2010). A new modeling approach for the study of finned coils with CO2. *International Journal of Thermal Sciences, 49*(9), 1702-1711. doi: DOI 10.1016/j.ijthermalsci.2010.04.002

Bredesen, A. M., Hafner, A., Pettersen, J., Neksa, P., & Aflekt, K. (1997). Heat transfer and pressure drop for in-tube evaporation of CO2. *Heat Transfer Issues in Natural Refrigerants, 1997*(5), 35-49.

Cavallini, A., Cecchinato, L., Corradi, M., Fornasieri, E., & Zilio, C. (2005). Two-stage transcritical carbon dioxide cycle optimisation: A theoretical and experimental analysis. *International Journal of Refrigeration-Revue Internationale Du Froid, 28*(8), 1274-1283. doi: DOI 10.1016/j.ijrefrig.2005.09.004

Chen, Y., & Gu, J. J. (2005). The optimum high pressure for CO2 transcritical refrigeration systems with internal heat exchangers. *International Journal of Refrigeration-Revue Internationale Du Froid, 28*(8), 1238-1249. doi: DOI 10.1016/j.ijrefrig.2005.08.009

Deng, J. Q., Jiang, P. X., Lu, T., & Lu, W. (2007). Particular characteristics of transcritical CO2 refrigeration cycle with an ejector. *Applied Thermal Engineering, 27*(2-3), 381-388. doi: DOI 10.1016/j.appthermaleng.2006.07.016

Falex Corporation. *Bulletin Number:QG-18. Pin & Vee Block Test Machine*.

Fenghour, A., Wakeham, W. A., & Vesovic, V. (1998). The viscosity of carbon dioxide. *Journal of Physical and Chemical Reference Data, 27*(1), 31-44.

Goodman, C., Fronk, B. M., & Garimella, S. (2011). Transcritical carbon dioxide microchannel heat pump water heaters: Part II - System simulation and optimization. *International Journal of Refrigeration-Revue Internationale Du Froid, 34*(4), 870-880. doi: DOI 10.1016/j.ijrefrig.2010.12.001

Halozan, H., & Ritter, W. (1994). Transcritical CO2 – a New Cycle. Austrial proposal for the working COHEPS Meeting, Trondheim, Norway.

He, M. (2012). *Numerical Modeling of Geothermal Borehole Heat Exchanger Systems.* (PhD), De Montfort University, Leicester, UK.

Jensen, M. K., & Jackman, D. L. (1984). Prediction of Nucleate Pool Boiling Heat-Transfer Coefficients of Refrigerant-Oil Mixtures. *Journal of Heat Transfer-Transactions of the Asme, 106*(1), 184-190.

Jin, Z., Eikevik, T. M., Neksa, P., Hafner, A., Ding, G., & Hu, H. (2014). *Transient Simulation of R744 Hybrid Ground Coupled Heat Pump with Modelica*. Paper presented at the 11th IIR Gustav Lorentzen Conference on Natural Refrigerants Hangzhou, China.

Kim, M. H., & Bullard, C. W. (2001). Development of a microchannel evaporator model for a CO2 air-conditioning system. *Energy, 26*(10), 931-948. doi: Doi 10.1016/S0360-5442(01)00042-1

Kim, M. H., Pettersen, J., & Bullard, C. W. (2004). Fundamental process and system design issues in CO2 vapor compression systems. *Progress in Energy and Combustion Science, 30*(2), 119-174. doi: DOI 10.1016/j.pecs.2003.09.002

Kim, S. C., Won, J. P., & Kim, M. S. (2009). Effects of operating parameters on the performance of a CO(2) air conditioning system for vehicles. *Applied Thermal Engineering, 29*(11-12), 2408-2416. doi: DOI 10.1016/j.applthermaleng.2008.12.017

Kim, S. G., Kim, Y. J., Lee, G., & Kim, M. S. (2005). The performance of a transcritical CO2 cycle with an internal heat exchanger for hot water heating. *International Journal of Refrigeration-Revue Internationale Du Froid, 28*(7), 1064-1072. doi: DOI 10.1016/j.ijrefrig.2005.03.004

Klöcker, K., Flacke, N., & Schmidt, E. L. (1998). Energetische Bewertung konventioneller und transcritischer Kaltdampfkompressionsprozesse. Report, Kohlendioxid, Besonderheiten und Einsatzchancen als Kältemittel, Statusbericht des DKW No. 20, ISBN 3-932715-00-4.

Kornhauser, A. A. (1990). The Use of an Ejector in a Geothermal Flash System. *Proceedings of the 25th Intersociety Energy Conversion Engineering Conference, Vols 1-6*, 79-84.

Li, D. Q., & Groll, E. A. (2005). Transcritical CO(2) refrigeration cycle with ejector-expansion device. *International Journal of Refrigeration-Revue Internationale Du Froid, 28*(5), 766-773. doi: DOI 10.1016/j.ijrefrig.2004.10.008

Liao, S. M., & Zhao, T. S. (2002). Measurements of heat transfer coefficients from supercritical carbon dioxide flowing in horizontal mini/micro channels. *Journal of Heat Transfer-Transactions of the Asme, 124*(3), 413-420. doi: Doi 10.1115/1.1423906

Liao, S. M., Zhao, T. S., & Jakobsen, A. (2000). A correlation of optimal heat rejection pressures in transcritical carbon dioxide cycles. *Applied Thermal Engineering, 20*(9), 831-841. doi: Doi 10.1016/S1359-4311(99)00070-8

Lorentzen, G. (1990). Trans-critical vapour compression cycle device. International Patent Publication WO 90/07683

Lorentzen, G. (1995). The Use of Natural Refrigerants - a Complete Solution to the Cfc/Hcfc Predicament. *International Journal of Refrigeration-Revue Internationale Du Froid, 18*(3), 190-197. doi: Doi 10.1016/0140-7007(94)00001-E

Ma, Y. T., Liu, Z. Y., & Tian, H. (2013). A review of transcritical carbon dioxide heat pump and refrigeration cycles. *Energy, 55*, 156-172. doi: DOI 10.1016/j.energy.2013.03.030

Neksa, P. (2002). CO2 heat pump systems. *International Journal of Refrigeration-Revue Internationale Du Froid, 25*(4), 421-427. doi: Doi 10.1016/S0140-7007(01)00033-0

Oh, H. K., & Son, C. H. (2010). New correlation to predict the heat transfer coefficient in-tube cooling of supercritical CO2 in horizontal macro-tubes. *Experimental Thermal and Fluid Science, 34*(8), 1230-1241. doi: DOI 10.1016/j.expthermflusci.2010.05.002

Oritz, T., Li, D., & Groll, E. (2003). Evaluation of the performance potential of CO2 as arefrigerant in air-to-air air conditioners and heat pumps: system modeling and analysis. Final Report. ARTI.

Pettersen, J. (2002). *Flow visualization of CO_2 in microchannel tubes.* (PhD), Norwegian University of Science and Technology, Norway.

Pettersen, J., Hafner, A., Skaugen, G., & Rekstad, H. (1998). Development of compact heat exchangers for CO2 air-conditioning systems. *International Journal of Refrigeration-Revue Internationale Du Froid, 21*(3), 180-193. doi: Doi 10.1016/S0140-7007(98)00013-9

Richter, C. C. (2008). Proposal of New Object-Oriented Equation-Based Model Libraries for Thermodynamic Systems: Technische Universität Carolo-Wilhelmina zu Braunschweig.

Rieberer, R. (1998). *CO_2 as working fluid for heat pumps.* (PhD), Graz University, Austria.

Robinson, D. M., & Groll, E. A. (1998). Efficiencies of transcritical CO2 cycles with and without an expansion turbine. *International Journal of Refrigeration-Revue Internationale Du Froid, 21*(7), 577-589. doi: Doi 10.1016/S0140-7007(98)00024-3

Sarkar, J. (2008). Optimization of ejector-expansion transcritical CO2 heat pump cycle. *Energy, 33*(9), 1399-1406. doi: DOI 10.1016/j.energy.2008.04.007

Sarkar, J., Bhattacharyya, S., & Gopal, M. R. (2004). Optimization of a transcritical CO2 heat pump cycle for simultaneous cooling and heating applications. *International Journal of Refrigeration-Revue Internationale Du Froid, 27*(8), 830-838. doi: DOI 10.1016/j.ijrefrig.2004.03.006

Sarkar, J., Bhattacharyya, S., & Gopal, M. R. (2005). Transcritical CO2 heat pump systems: exergy analysis including heat transfer and fluid flow effects. *Energy Conversion and Management, 46*(13-14), 2053-2067. doi: DOI 10.1016/j.enconm,an.2004.10.022

Span, R., & Wagner, W. (1996). A new equation of state for carbon dioxide covering the fluid region from the triple-point temperature to 1100 K at pressures up to 800 MPa. *Journal of Physical and Chemical Reference Data, 25*(6), 1509-1596.

Srinivasan, K., Sheahen, P., & Sarathy, C. S. P. (2010). Optimum thermodynamic conditions for upper pressure limits of transcritical carbon dioxide refrigeration cycle. *International Journal of Refrigeration-Revue Internationale Du Froid, 33*(7), 1395-1401. doi: DOI 10.1016/j.ijrefrig.2010.06.009

Vesovic, V., Wakeham, W. A., Olchowy, G. A., Sengers, J. V., Watson, J. T. R., & Millat, J. (1990). The Transport-Properties of Carbon-Dioxide. *Journal of Physical and Chemical Reference Data, 19*(3), 763-808.

Yang, H., Cui, P., & Fang, Z. (2010). Vertical-borehole ground-coupled heat pumps: A review of models and systems. *Applied Energy, 87*(1), 16-27. doi: DOI 10.1016/j.apenergy.2009.04.038

Yang, J. L., Ma, Y. T., & Liu, S. C. (2007). Performance investigation of transcritical carbon dioxide two-stage compression cycle with expander. *Energy, 32*(3), 237-245. doi: DOI 10.1016/j.energy.2006.03.031

Yang, W., Fartaj, A., & Ting, D. (2005). CO2 automotive A/C system optimum high pressure control. SAE 2005-2001-2022.

Yin, H. M., Bullard, C. W., & Hrnjak, P. S. (2001). R-744 gas cooler model development and validation. *International Journal of Refrigeration-Revue Internationale Du Froid, 24*(7), 692-701.

Yoon, S. H., Kim, J. H., Hwang, Y. W., Kim, M. S., Min, K., & Kim, Y. (2003). Heat transfer and pressure drop characteristics during the in-tube cooling process of carbon dioxide in the supercritical

region. *International Journal of Refrigeration-Revue Internationale Du Froid, 26*(8), 857-864. doi: Doi 10.1016/S0140-7007(03)00096-3

Yun, R., Kim, Y. C., & Park, C. (2007). Numerical analysis on a microchannel evaporator designed for CO2 air-conditioning systems. *Applied Thermal Engineering, 27*(8-9), 1320-1326. doi: DOI 10.1016/j.applthermaleng.2006.10.036

Zhang, X. P., Fan, X. W., Wang, F. K., & Shen, H. G. (2010). Theoretical and experimental studies on optimum heat rejection pressure for a CO2 heat pump system. *Applied Thermal Engineering, 30*(16), 2537-2544. doi: DOI 10.1016/j.applthermaleng.2010.07.003